

https://dspace.org/

Gas recovery modelling of South African shale gas reservoir

Ogojiaku, Gertrude Obiageli

2022

https://hdl.handle.net/10539/34930

Downloaded from a DSpace repository. https://dspace.org/

Gas Recovery Modelling of South African Shale Gas Reservoir

Prepared by

Gertrude O. Ogojiaku, 2409922

A Research Report submitted to

The School of Chemical and Metallurgical Engineering, Faculty of Engineering and the Built Environment, University of the Witwatersrand, Johannesburg, South Africa, in partial fulfilment of the requirements for the Degree of Master of Science in Petroleum Engineering.

Supervisor: Dr. Diakanua Nkazi

August 2022

i) Plagiarism declaration

This section serves to confirm that the work presented herein is the product of the author(s).

Any work that has been adopted from other sources has been referenced.

No work from other sources has been presented without acknowledgement.

No one has been allowed to copy the work presented in this document.

Signature: _____ Date: August 2022

Abstract

As the production of shale gas increases globally, there are various mechanisms that are displayed through the flow of shale gas to the wellbore, this creates a prompt for the shale reservoir behavior to be developed for a better comprehension on the complexities of the shale layer. Shale gas cannot be produced naturally as they exist in tight pores. Therefore, to increase productivity, shale gas is extracted through the means of horizontal drilling or hydraulic fracturing, commonly known as fracking. The triple porosity model in this paper considers three different but consecutive flows in the shale layer from the Matrix, Natural Fracture and Hydraulic Fracture. This paper discusses the flow properties of shale gas reservoirs, developing mathematical flow models and how these models can be efficient in predicting recovery of shale gas in South Africa in comparison to existing shale gas reservoirs.

The flow equations at the systems were developed and solved using the Finite Difference Method. Once solved explicitly, using MATLAB, the algorithm was plotted to illustrate the reservoir pressure distribution with respect to time.

In conclusion, the analysis of the results shows that the behavior of the reservoir with regards to pressure and time is in line with previously simulated triple porosity models done by other researchers. This demonstrates the closeness in behavior of the developed model in this research and renders it viable for use in any reservoir to be effective in predicting the production of shale gas.

Table of Contents

i) Plagiarism declaration i

Abstract ii

List of Figures v

List of Tables vi

Nomenclature vii

Acknowledgments viii

Chapter 1: INTRODUCTION 9

1.1 Shale Gas Reserves Location in South Africa 9

1.2 Shale Gas Extraction Method 10

1.3 Aim and Objectives 11

Chapter 2: LITERATURE REVIEW 12

2.1 Shale - The Host Rock 14

2.2 Shale Gas Extraction 15

2.2.1 Stages of Shale Gas Extraction 15

2.3 Hydraulic Fracturing 16

2.4 Dual Porosity Model 17

2.5 Triple Porosity Model 18

Chapter 3: FLOW CHARACTERISTICS OF SHALE GAS RESERVOIR 20

3.1 Darcy and Non Darcy Flow 20

3.2 Adsorption and Desorption Mechanism 22

3.3 Knudsen Number 24

Chapter 4: MATHEMATICAL MODEL CONSTRUCTION 27

4.1 Model Assumptions 27

4.2 The Flow Equation of The Matrix Phase 27

4.3 The Flow Equation of The Natural Fractures 31

4.4 The Flow Equation of The Hydraulic Fracture 33

Chapter 5: METHODS USED IN SOLVING FLOW EQUATIONS 35

5.1 Finite Difference Method 35

5.2 Finite Element Method 36

5.3 Solution to Developed Model 36

5.3.1 Hydraulic Fracture Phase 37

5.3.2 Natural Fracture Phase 38

5.3.3 Matrix Phase 39

Chapter 6: RESULTS AND DISCUSSION 41
6.1 Matrix Phase 41
6.2 Natural Fractures 43
6.3 Hydraulic Fractures 46
Chapter 7: CONCLUSION 53
REFERENCES 54
Appendices 60
Appendix A 60
Appendix B 62
Appendix C 63

List of Figures

Figure 1.1: Map showing the geology timescale of the Karoo Basin in South Africa 9

Figure 2.1: An illustration of hydraulic fracturing. 15

Figure 2.2: Heterogeneous dual-porosity reservoir. 16

Figure 3.1: A model showing the transport of methane in a fracture network, a) reservoir with hydraulic fractures, b) flow transport within the fracture network 19

Figure 3.2: Schematic showing gas diffusion from the Kerogen to the pores in the shale matrix a) SEM image of the kerogen system b) microscopic sketch of the kerogen system 21

Figure 3.3: Schematic showing different flow regimes of shale gas transport mechanism 23

Figure 6. 1: Reservoir pressure distribution in the matrix pores against time 41

Figure 6.2: Reservoir pressure distribution in the natural fractures against time with u (1,j,k)=300x(k<12)+70 43

Figure 6.3: Reservoir pressure distribution in the natural fractures against time without u (1,j,k)=300x(k<12)+70 44

Figure 6.4: Reservoir pressure distribution in the hydraulic fractures against time 46

Figure 6.5: Reservoir pressure distribution in the hydraulic fractures against time 47

Figure 6.6: Pressure behavior in the hydraulic fractures against time where the constant b is 0.18 .. 48

Figure 6.7: Pressure behavior in the hydraulic fractures against time where the constant b is 0.13 .. 49

Figure 6.8: Pressure behavior in the hydraulic fractures against time where the constant b is 0.11 .. 50

Figure 6.9: Pressure behavior in the hydraulic fractures against time where the constant b is 0.05 .. 51

Figure A: Coding of the matrix phase equation using MATLAB 61

Figure B: Coding of the natural fractures equation using MATLAB 62

Figure C: Coding of the hydraulic fractures equation using MATLAB 63

List of Tables

Table 1. 1: Petro-physical rock properties of the Southern Karoo Basin in South Africa 12
Table 1. 2: Provisional data applied during simulation..... 13

Nomenclature

	Units	Symbol
Natural fracture		NF
Hydraulic fracture		HF
Reservoir thickness	m	h
Reservoir length,	m	L
Reservoir breadth	m	w
Klinkenberg coefficient	MPa	b
Matrix porosity,		ϕ_m
Natural fracture porosity,		ϕ_{NF}
Hydraulic fracture porosity,		ϕ_{HF}
Compressibility factor,		Z
Normal direction		n
Wellbore radius,	m	r_w
Initial reservoir pressure	Pa	p_i
Bottom-hole pressure	Pa	p_w
Matrix pressure	Pa	p_m
Natural fracture pressure	Pa	p_{NF}
Hydraulic fracture pressure	Pa	p_{HF}
Langmuir pressure	Pa	p_L
Reservoir temperature	K	T
Langmuir volume,	m^3/kg	V_L
Apparent permeability	m^2	k_a
Intrinsic permeability	m^2	k_l
Matrix apparent permeability	m^2	k_{ma}
Natural fracture absolute permeability	m^2	k_{NF}
Absolute permeability of hydraulic fracture	m^2	k_{HF}
Molecular weight of gas	kg/mol	M
Interface area per unit volume of rock	m^{-1}	$A_{m\rightarrow NF}$
Interface area per unit volume of rock	m^{-1}	$A_{NF\rightarrow HF}$
Gas Viscosity	cP	μ_g
Universal gas constant	[Pa m^3/(kmol .K)]	R
Gas density	(kg/m^3)	ρ
Time	(s)	t
Langmuir volume	(m^3/m^3)	V_L
Adsorbed gas content	(m^3/m^3)	V_E

Acknowledgments

I would like to give all the glory to God Almighty who not only ordained me with this course but also guided me through this research till the very end.

Thank you to my amazing family and friend, Erezimena whose support, prayers and encouragement never ceased and in turn contributed to my zeal to keep going during this research, you all are my light.

A very special appreciation goes out to my supervisor Dr. Diakanua Nkazi, despite all you had on your plate you never hesitated to help and stir me in the right direction. You provided me with resources, guidance, and support and for that I am entirely grateful. Thank you for the opportunity to have worked with you during this research.

To Dr. Stephanie Enslin, thank you for your guidance, resources, support and encouragement. You patiently showed me the ropes and took the time to correct my submissions.

Lastly, I would like to thank myself with a huge pat on the back for keeping it going through what I may call the toughest year of my life and finally seeing my courses and this research through with the special Grace of God.

Chapter 1 INTRODUCTION

The main source of energy on a global scale are fossil fuels (oil & gas), accounting for 81% of global primary energy use in 2010 (IEA, 2011). Therefore, this prompts the need to exploit unconventional energy resources as energy usage rises (UNEP, 2011a, b) and conventional reserves are depleting (IEA, 2010). Unconventional gas, such as shale gas is increasingly playing a role in the future growth of gas reserves and output around the world, particularly in developed countries like United States of America, China, Canada and Argentina which are the top countries that have realized commercial development of shale gas (EIA 2016). Recently South Africa has been the focus of shale gas interests entrapped in shales of the Karoo Basin in the province of the Eastern and Western Cape, and thus has been identified as a significantly potential area to extract and explore shale gas (Geel, et al., 2013).

1.1 Shale gas reserves location in South Africa

The Karoo Basin is said to comprise 75% of the entire country (McCarthy and Rubidge, 2005). The Western and Eastern Cape region is rich in shales particularly the Prince Albert Formation, which consists of mudstone with shale and deposits of sandstone, and Whitehill Formation which consists of fine-grained, black organic rich shale, and both shale layers occur in the deeper, south region of the basin. These shales pinch out further north between Hertzogville in the northwest and Coffee Bay in the southeast (Cole et al. 2011). Researchers have estimated the shale gas deposits to be 450 Tcf (trillion cubic feet). Further studies taking into account dolerite intrusions have provided more ranges for the reserves between 14-172 Tcf (Decker and Manor, 2012) and 10 to 50 Tcf (Chere et al., 2017) for the shales around the Southern region. These studies considered different size regions (Chere et al, 2017) including the south-central Karoo Basin southeastwards

to East London. The gas reserves were estimated at 65 to 400 Tcf in the Upper Ecca shales. (Chere et al, 2017).

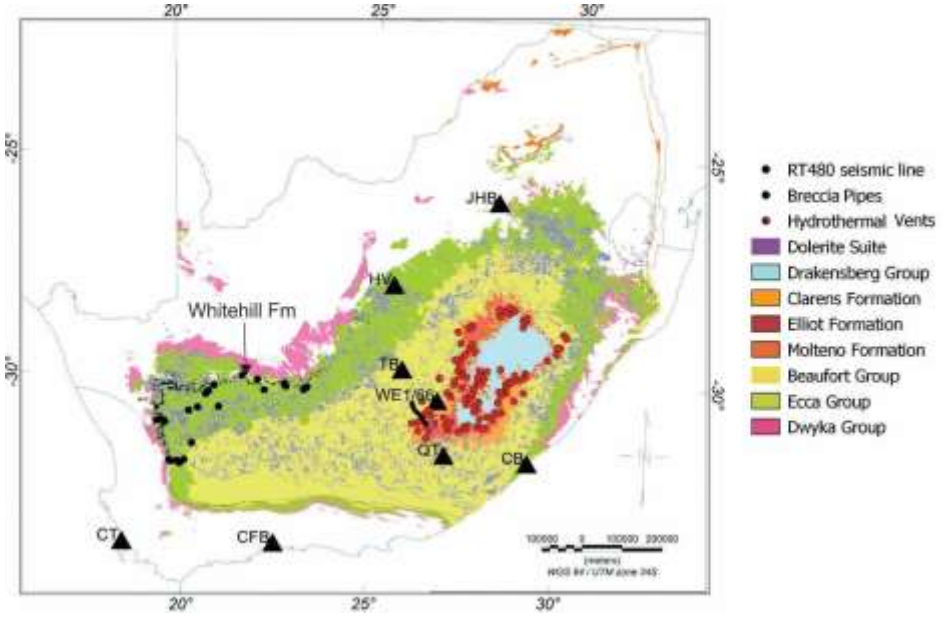


Figure 1.1 Map showing the geology timescale of the Karoo Basin in South Africa (Scheiber-Enslin, Manzi & Webb, 2021)

1.2 Shale gas extraction method

Hydraulic fracturing is a method used in extracting gas from low permeable tight shale layers (Boyer, et al., 2011). Unconventional gas generally comprises of methane (CH4), and it is extracted through the process of fracking (Boyer, et al., 2011). Horizontally drilled wells and high volume of hydraulic fracturing methods are employed to increase production of natural gas (Vengosh, et al., 2014). A hydraulic fracture is formed by pumping millions of liters of water, fracturing fluid into a wellbore at a rate sufficient to increase pressure at the target depth (determined by the location of the well casing perforations), to exceed that of the fracture gradient (pressure gradient) of the rock. This enables the trapped natural gas to flow out of the tight rock

layers through the well and is then extracted at the top of the well. (Jackson, et al., 2014). During the course of this paper, the method of shale extraction will be described in the next chapter.

The successful exploration of shale gas relies greatly on fractures, especially hydraulic fractures created during fracking. These fractures affect the flow of gas, which can be modelled and ultimately impacts production. The shale reservoir can have different flow system, namely flow within the matrix phase, flow within natural fractures and flow through hydraulic fractures created during fracking. These various flow systems affect the production of shale gas reservoirs due to factors such as permeability, porosity, and transient pressure.

1.3 Aim and Objectives

The aim of this proposed study is to develop a gas recovery mathematical model which accounts for the flow of shale gas from the reservoir to the wellbore using data from the South African Karoo Basin.

The following objectives will be undertaken during the course of the study;

- To develop a triple continuum model with three system flows (matrix – natural fracture – hydraulic fracture).
- To validate the model with field parameters gotten from published reservoirs containing shale gas.
- To analyze the effect of pressure and permeability on the recovery process.

Chapter 2 LITERATURE REVIEW

Many researchers have developed models and published articles describing multiple stages of flow in a shale gas reservoir (Guo & Wei, 2015; Ahmadi and Ershaghi, 1996). These various flow systems affect the production of shale gas reservoirs due to factors such as permeability, porosity, and transient pressure. Several studies have considered flows at different media such as; micropore, mesopore, macropore, matrix, microfracture, macro fracture, natural fracture, hydraulic fracture and adsorbed gas, however, some factors (desorption, diffusion, kerogen bulk, slip flow in nanopores within matrix) failed to be considered and as such affect the accurate recovery of shale reservoirs. This work will focus on predicting the South African shale gas reservoir to determine potential gas recovery by validating the model created with an existing shale gas reservoir. Data collected from the KWV-1 borehole as well as data from (Jiang & Xu, 2017; Guo & Wei, 2015) where KWV-1 is insufficient will be used to develop a model for prediction. These parameters are listed in Tables 1.1 and 1.2.

Table 1.1 Petro physical rock properties of the southern Karoo Basin, South Africa (Campbell, et al., 2016)

Sample location	KWV-1 (Borehole)	Ecca pass
Number of measurements	32	76
Density range(kg/m3)	2570-2770	2630-2730
Density mean(kg/m3)	2700	2670
Porosity range	0.4-2.2	0-3.7
Porosity mean	1.3	1
Permeability (mD) range	0.001-0.002	0.01-0.1
Permeability (mD) mean	0.05	0.0014

Table 1.2 Provisional data applied during simulation (Guo et al., 2015; Zhang et al,. 2016)

Parameter	Symbol	Value	Units
Reservoir length,		1300	m
Reservoir breadth		600	m
Effective thickness		2	m
Fracture half-length		146	m
Fracture spacing	r_e	200	m
Wellbore radius	r_w	0,1	m
Initial reservoir pressure	p_i	20	MPa
Bottom-hole pressure	p_w	5	MPa
Initial reservoir temperature	T	350	K
Langmuir pressure	p_L	5	MPa
Langmuir volume	V_L	1	m^3/m^3
Porosity of the matrix phase	ϕ_m	0,05	
Porosity of the Natural phase	ϕ_{NF}	0,01	
Porosity of the hydraulic phase	ϕ_{HF}	1	
Matrix permeability	k_{ma}	0,00005	mD
Natural fracture permeability	k_{NF}	0,05	mD
Hydraulic fracture permeability	k_{HF}	8000	mD
NF interface area per unit volume of rock	α_{NF}	50	m^{-1}
HF interface area per unit volume of rock	α_{HF}	0,5	m^{-1}
NF Characteristic length,	L_{NF}	0,1	m
HF Characteristic length,	L_{HF}	1	m
Skin Factor	S	1	
Gas Viscosity,	μ_g	$1.265x10^{-5}$	Pa.s
Standard molar volume	V_{std}	22,414	m3/kmol
Molecular Weight	MW	16	kg/kmol

2.1 Shale – The Host Rock

Shale is a heterogeneous and anisotropic porous material. It contains inorganic matter such as clay minerals (montmorillonite, chlorite, kaolinite, and illite), calcite, pyrite, quartz and organic matter (kerogen) (Wang F, Reed R, 2009). Black shale consists of large amounts of organic materials that are developed by deep burial which increases their compaction, and with reduced porosity at a certain temperature and pressure can generate oil and natural gas entrapped within its pores (Blatt, Harvey et al., 1996; Tissot and Welte, 1984; Wilde et al., 2004; Azah Abanda and Hannigan, 2006; Aguilera et al., 2014). The source rock which produces the gas in shale gas contains low permeable and porous reservoir properties (Suarez-Ruiz et al., 2012). The trapping mechanism involved in the self-sourced hydrocarbon resource extends widely and is therefore classified as conventional (Curtis, 2002; Zou et al., 2014). The gas within the natural fractures is considered dry, containing more than 90% methane, or wet with longer-chained hydrocarbons such as ethane and propane (Chere et al, 2017). The formation of natural gas in shale is affected by various conditions and components, hence not all shale formations contain considerable amount of gas for exploitation. For example, the shale must contain rich amounts of organic properties which will allow the shale to be more breakable, this would be advantageous to the reaction of the rock layers to hydraulic simulation (EIA/ARI, 2013). In opposition, shale layers with low quartz content would be less flexible and unbreakable thereby being more resistant to fracking. Thermal maturation of shale gas is relatively large and is measured in high temperatures between (100 and 250°C; Tissot and Welte, 1984).

2.2 Shale Gas Extraction

Unconventional gas, i.e., shale gas, is trapped in low permeable rock formations and as such cannot escape freely after drilling, therefore a gas extraction technique must be applied in order to release the gas in commercial quantities.

2.2.1 Stages of Shale Gas Extraction

Shale gas extraction comprises of three stages:

- Exploration: This stage functions as a trial stage whereby vertical wells are drilled and fractured to check for the existence of shale gas that could be extracted. If shale gas is discovered, a little more observation would be carried out to determine if the shale gas is sufficient enough to be produced economically. Subsequently, more wells may be drilled to find out the economic longevity of the gas.
- Production: The commercial possibility of producing shale gas is evaluated at this stage. Typically, shales with high commercial quantities of gas are greater than a hundred metres thick and will continue across over hundreds of metres deeper. Such shales are considered to be naturally almost horizontal with shallow dips. During vertical drilling only a small amount of gas would be retrieved as the technique does not allow for enough recovery. After a vertical well has been drilled, the drill bit is then diverged horizontally. Horizontal wells are best preferred in recovering more gas for production.
- Abandonment: As it is common practice during oil and gas exploration, shale gas reservoirs are abandoned once its full production capacity is reached, and it declines in economic value. The well is then sectioned out and cemented to prevent flow of gas to the surface and water-bearing zones.

2.3 Hydraulic Fracturing

Hydraulic fracturing commonly referred to as fracking or hydrofracking is a well stimulation technique involving the injection of high-pressure liquid below the reservoir surface in order to breakdown entrapped gas and instigate free flow (Gandossi, Luca et al 2015). In the fracking process, once a well has been drilled and completed, electric currents which generates explosive charges is fired to create punctured holes along certain intervals of the well within the production zone of the shale layer. Fracturing fluids which are primarily water, containing sand or other proppants suspended with the help of thickening agents are injected into the well using pumps (Figure 2.1). The fracture penetrates into the shale layer by a few metres and fracking fluids are injected to maintain the reservoir pressure in order for fracturing to continue at a deeper level of the rock (API 2009). Plugs are used to divide the well into several stages so that reservoir pressure can be optimized.

After fracturing, the plugs are perforated so that the well is depressurized. This creates a change in pressure to enable the shale gas flow out of the shale. During hydraulic fracturing, fracking fluid and fluids mixed with saline and dissolved minerals returns to the surface over the lifetime of the well as it continues to produce shale gas. Flow back water and produced water are classified as wastewaters and are therefore treated to minimize environmental impacts (EPA 2011).

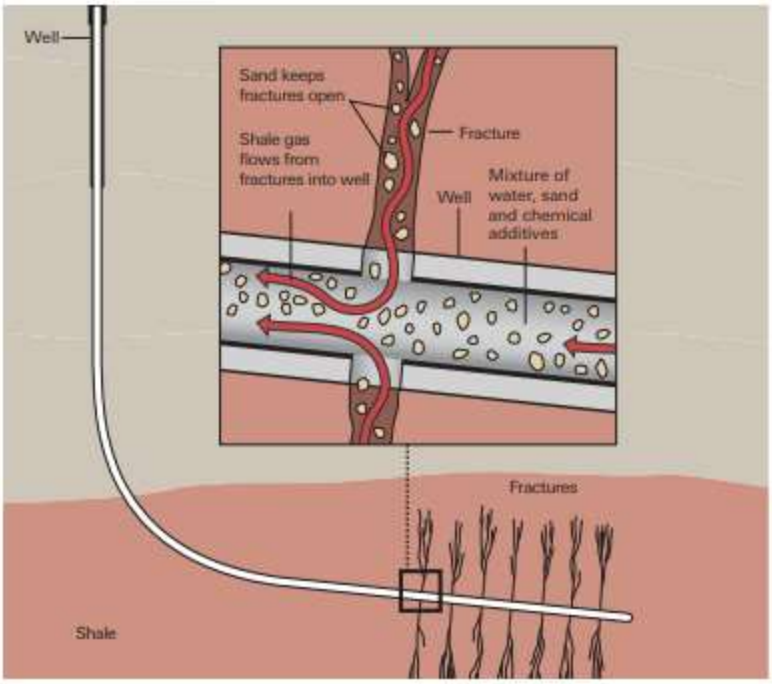


Figure 2.1 An illustration of hydraulic fracturing (Sutter, Lori & Weston et al, 2015)

2.4 Dual Porosity Model

Dual porosity model is mostly used when simulating fluid flow for naturally fractured reservoirs. The model was originally proposed by Warren & Root (1963) (Figure 2.2) who assumed a pseudo steady-state fluid transferred between the matrix phase and natural fractures. An unsteady state (transient) was also assumed to flow between the matrix and fractures (Kazemi 1969, De Swaan 1976, and Ozkan et al 1987).

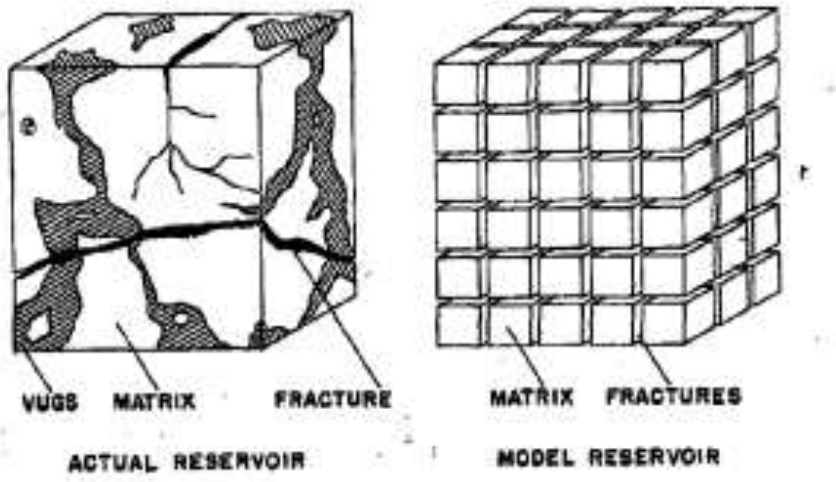


Figure 2.2 Heterogeneous dual-porosity reservoir (Warren, 1963)

2.5 Triple Porosity Model

The diffusion and adsorption aspect of shale gas reservoirs are mostly neglected in dual porosity models, and it was discovered that they may not be accurate in simulating real-life reservoirs. Therefore, an improvement to the drawbacks were realized and a triple porosity model was formed which considers two different fracture systems with different properties. Abdassah and Ershaghi (1986) instituted the first triple porosity model then Ahmadi and Ershaghi (1996), Drier (2004), and several others further continued to improve the originally proposed models. The triple porosity model captures the reservoir heterogeneity by subdividing each medium and assigning each one with different properties by considering the fact that the fractures consist of unique properties (Al-Ahmadi HA 2010). In an effort to determine the transient pressure below the surface of the shale layer, triple continuum models are proposed to be solved using a numerical method approach as opposed to an analytical approach which was mostly used by previous researchers. The transport of gas by the diffusion mechanism which has been proven to have a significant impact on gas flow

and diffusion therefore need to be considered in the production simulation of fractured shale gas reservoirs.

Chapter 3 FLOW CHARACTERISTICS OF SHALE GAS RESERVOIR

Shale gas flow is different from conventional gas flow and cannot be produced naturally as they exist in tight pores (Zhang, Jiang, Lu, et al 2017). The many different physical properties and flow mechanisms that occur within the shale layer and hydraulically fractured wells will be discussed in this chapter.

3.1 Darcy and Non-Darcy Flow

Due to the storage of gas existing in a free and absorbed form during shale gas exploration, it is significant to understand the different flow regimes. Darcy's flow cannot fully describe the transport of gas in a porous media, therefore, the transition of gas flow for Darcy to Non-Darcy flow poses an effect on shale gas transport. Several gas properties can affect the flow of gas on a nanoscale and as a result, Darcy's equation may be derived as insufficient (Swami et al, 2012). The flow of gas in this system can either be Darcy or non-Darcy flow, depending on the rate at which the gas is channelled and the Reynold's number of the gas (Berawala, 2015).

In Figure 3.1, the flow of gas in fractured gas reservoirs is described. The flow systems in a fractured gas reservoir exist as a form of viscous flow and the transmission of gas within both fractures.

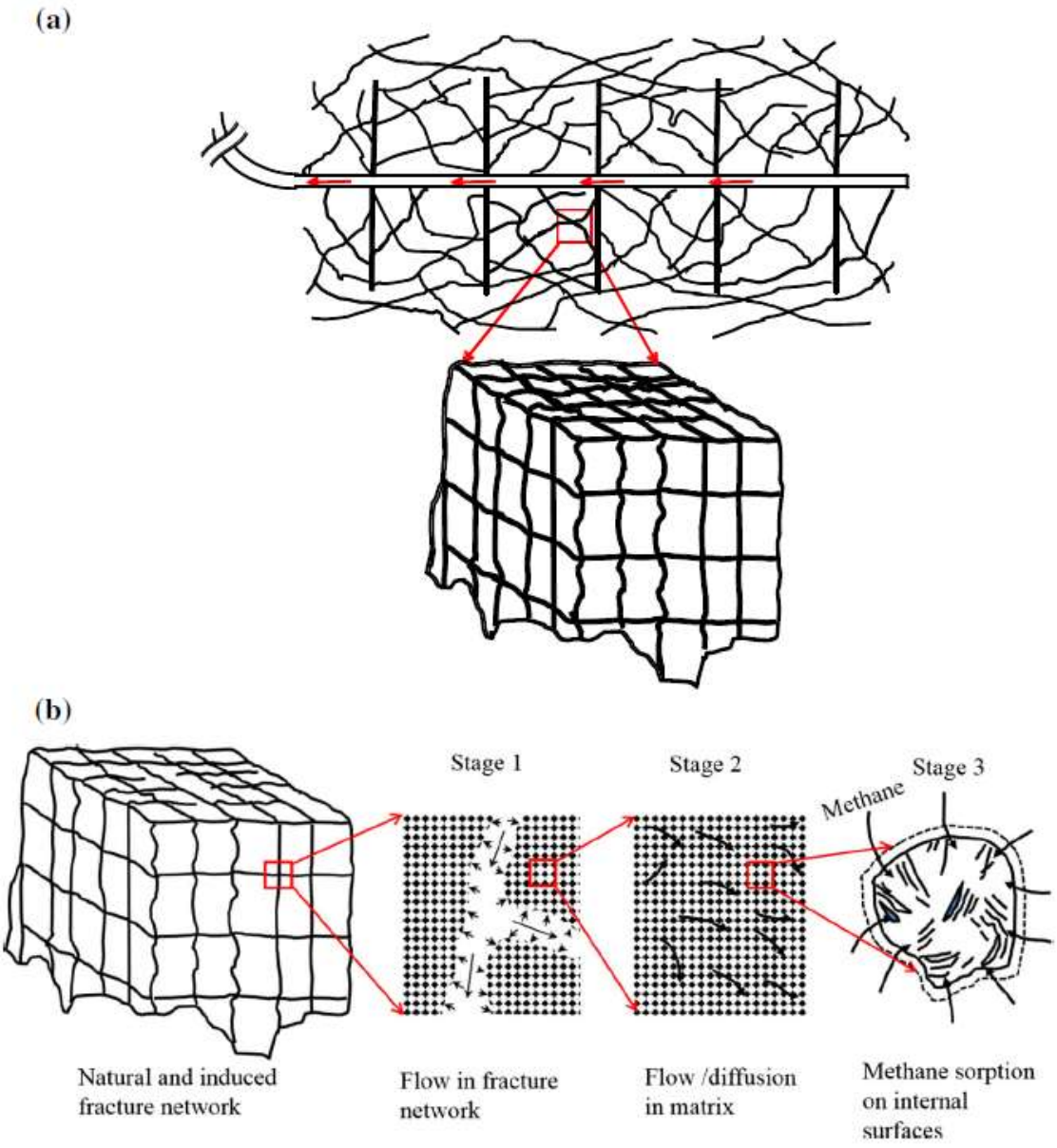


Figure 3.1 A model showing the transport of methane in a fracture network, **a**) reservoir with hydraulic fractures, **b**) flow transport within the fracture network

The original accumulated gas within the matrix transforms into a freed gas as a decline in pore pressure occurs. The freed gas existing is then distributed within the matrix grids and slowly accumulates into the fracture system. Afterwards, the accumulated gas flows out of the matrix into

the fracture system and then above the well surface (Bustin and Bustin 2012; Wang et al. 2012; Wang 2014; Yu and Sepehmoori 2014). Essentially, several flow mechanisms direct the transport of gas in respective medias. For instance, in the fracture network, the passage of gas is typically represented in the form of Darcy or non-Darcy law as a result of the gas viscosity. However, the flow within the shale matrix displays a more intricate mechanism which is generally regarded as an irregular transmission mechanism that varies due to the pore pressure.

3.2 Adsorption and Desorption Mechanism

The presence of gas in a shale reservoir exists in three states: free gas, adsorbed gas or dissolved gas (Pollastro, 2007). According to past studies, the main state of gas present in shale layer amongst the three listed states above is adsorbed gas which ranges between 20% - 80% of accumulated gas within the reservoir (Lu, Li & Watson, 2010). To optimize hydraulic fractures and characterize shale structures, adsorption properties can give a more analytical overview in this approach. Eventually, due to a decrease in environmental pressure, adsorbed gas will be released to form part of free gas during early stages of production (Grieser, Shelley and Soliman, 2009). For this reason, the importance of adsorption/desorption in regard to forecasting well production cannot be overemphasized. Several studies have managed to examine the methane adsorption mechanisms (Zhang, Ellis, Ruppel, 2012). According to some reviews, the main source of adsorption on a shale surface is regarded as molecular accumulation (Zhang and Yang, 2012). This is due to the minimization theory of surface energy (Zhang and Yang, 2012), however actual model is occasionally considered in identifying the adsorption process as the gas is held at the surface as a result of weak van der Waals forces which leads (Rexer et al, 2013). Recently, other reservoir properties such as temperature, pressure etc., have also been considered to affect the adsorption function (Tan et al., 2014). Total Organic Carbon is also a property with effect on the adsorption

capacity. Once there is an increased amount of total organic carbon content, it will reflect in value against the entire pore volume, porosity and area thereby indicating a high adsorption capacity as opposed to low TOC content. Shale rock contains high levels of organic matter compared to other rocks; thus, this results in a high amount of gas adsorption.

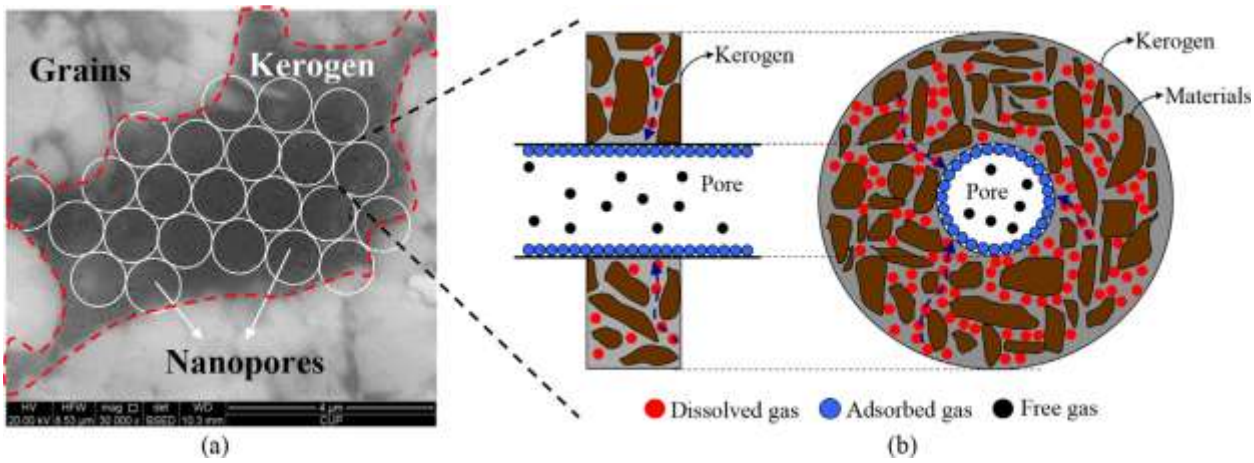


Figure 3.2 Schematic showing the gas diffusion from the kerogen to the pores in the shale matrix. **a**) SEM image of the kerogen system, **b**) microscopic sketch of the kerogen system (Mi, Jhiang and Li, 2014)

Desorption of gas from the organic matrix occurs when there is a decrease in pressure in the matrix during exploitation; this desorbed gas then functions as free gas within the matrix, and as a source of gas which feeds into the micro-fractures system (Berawala, 2015). This phenomenon is an equilibrium process whereby the difference in pressure will be formed between the matrix and the pores, thus pressure decreases as free gas is being produced and the desorption on the matrix surface is reinforced (Guo et al., 2014). Many equal or constant models have been used in defining gas adsorption, however the easiest and most effective of them all is Langmuir adsorption model (Tang et al., 2016).

The Langmuir isotherm is given by:

$$\text{Vads} = \text{VL} * \frac{\text{p}}{\text{P+ PL}} \qquad (3.1)$$

where Vads (kg/m^3) = Volume of gas adsorbed per unit mass in shale matrix

VL (kg/m^3) = The Langmuir volume

P (Pa) = The reservoir pressure

P_L (Pa) = The Langmuir pressure

In evaluating gas in place during production, it can be easily overestimated or underestimated due to the high assumption of the gas adsorption capacity. Enhanced models of the isotherm model have been used to describe the gas adsorption performance on the shale surface (Mertens, 2009). A commonly used model of the Langmuir isotherm is given as:

$$q_{ads} = \frac{\rho_s . M_g}{V_{std}} . \text{VL} * \frac{\text{p}}{\text{P+ PL}} \qquad (3.2)$$

where q_{ads} (kg/m^3) = The mass of adsorbed gas per solid volume

ρ_s (kg/m^3) = The material density of the shale matrix

M_g (kg/mol) = The molecular weight of shale gas

V_{std} (m^3/kmol) = Molar volume of shale gas at standard temperature and pressure, (273.15K and 101,325 Pa, respectively.

3.3 Knudsen Number

The flow mechanism that occurs within the surface of a shale layer has been described to exists on the within a porous media with several ranges of pore size from macroscale (> 1mm) to nanoscale

(< 100nm) (Di and Jensen, 2015). This description of several gas transports through different pore scale characteristics in the media are determined by Knudsen number.

Knudsen number is given as:

$$K_n = \frac{\lambda}{r} \qquad (3.3)$$

where λ = the mean free path of molecules

r = the pore characteristics length

Knudsen number is represented in four types: continuous flow ($K_n < 10^{-3}$), slip flow ($10^{-3} < K_n < 10^{0.1}$), transition flow ($0.1 < K_n < 10$) and Knudsen flow ($K_n > 10$), several reservoir conditions in terms of temperature and pressure play a role in the different flow regimes (Beskok, Karniadakis and Trimmer, 1996).

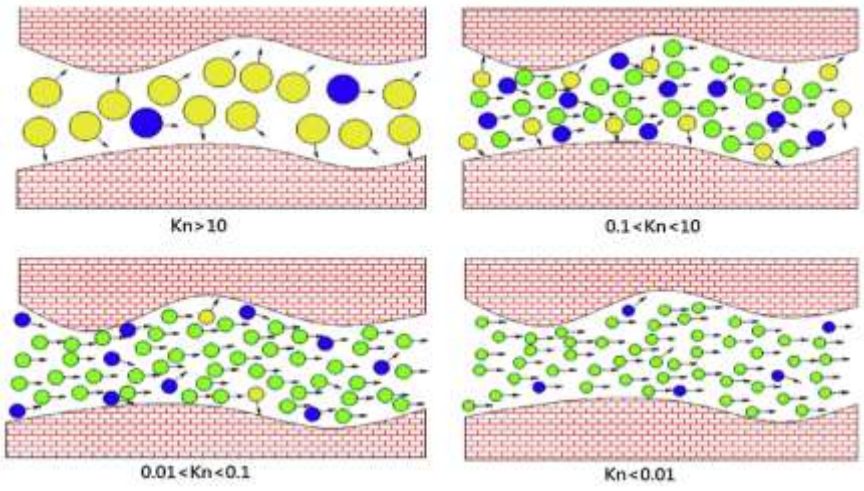


Figure 3.3 Schematic showing different flow regimes of shale gas transport mechanism (Song, Wang and Li, 2016)

This parameter quantifies the apparent gas permeability. The flow mechanism in organic rich shales exists in flow paths with adsorptive pore walls, therefore in determining apparent

permeability the decrease in volume that occurs within the adsorbed gas surface must be examined (Jiang and Younis, 2015). Due to the effect of different pore diameters, there is a slippage effect on gas flow which will change its regimes. Gas slippage effect has been used in a vast range of practices to describe transport properties of shale gas flow. In previous studies, the Klinkerberg factor has been applied in order to adjust permeability against gas slippage effect.

The apparent permeability is given by:

$$k_a = k_i \left(1 + \frac{b}{p}\right) \qquad (3.4)$$

Where k_a = the apparent permeability

k_i = the steady permeability

b = the Klinkerberg factor

And Klinkerberg factor, b is represented as:

$$b = \frac{4k_i}{2.81708k_i\sqrt{\frac{k_i}{\phi}}}\sqrt{\frac{\pi RT}{2MW_g}} \qquad (3.5)$$

Where ϕ = the rock porosity

R = the universal gas constant, given as 8.341 Pa m^3/kmol.K

T = the reservoir temperature in kelvin

Chapter 4 MATHEMATICAL MODEL CONSTRUCTION

4.1 Model Assumptions

1. The model incorporates three medias: Matrix, Natural Fractures and Hydraulic Fractures. The triple continuum model are three exclusive mediums which are interconnected via inter-porosity flow.
2. A continuous flow is assumed from Matrix – Natural Fractures – Hydraulic Fractures
3. The Matrix and Natural Fractures is considered two dimensional while the Hydraulic Fracture is considered one dimensional.
4. Desorption of adsorbed gas is considered in the Matrix and Klinkenberg factor is not altered in the Natural and Hydraulic Fractures.
5. The temperature in the reservoir is assumed to be constant.
6. Viscosity of gas is assumed to be constant.
7. No gravity effect is assumed.

4.2 The flow equation of the matrix phase

In this phase, free gas and adsorbed gas exists, hence the mass of gas can be represented as;

$$mass\ of\ gas\ in\ the\ matrix = free\ gas + adsorbed\ gas \qquad (4.1)$$

This is mathematically represented as,

$$mass\ of\ gas\ in\ the\ matrix = \rho_g \phi_m + \rho_g V_{ads} * \rho_s \qquad (4.2)$$

where ρ_g= density of gas, i.e., $\rho_g = \frac{pM}{zRT}$, (4.3)

M= the gas molecular weight

R= 8.314×10^3 (J/kmol.K)

The subscripts *g*, *m*, *NF*, and *HF* respectively symbolizes gas, matrix, natural fracture and hydraulic fracture in equations 4.2 and 4.3.

The mass of gas in the matrix will be derived through the rate of mass accumulation in respect to time,

$$\frac{\partial}{\partial t}\left(\rho_g\phi_m + \rho_g V_{ads} * \rho_s\right) = \frac{\partial}{\partial t}\left(\frac{pM}{zRT}\phi_m\right) + \frac{\partial}{\partial t}\left(\rho_g V_{ads} * \rho_s\right) \qquad (4.4)$$

$\frac{\partial}{\partial t}\left(\rho_g V_{ads} * \rho_s\right)$ represents the rate of adsorbed gas with time per shale matrix volume, this is therefore represented as

$$\frac{\partial}{\partial t}\left(\rho_g V_{ads} * \rho_s\right) = \frac{\partial q_{ads}}{\partial t} = \frac{\rho_s M}{V_{std}} * VL * \mathrm{PL} * \frac{1}{(\mathrm{P}+\mathrm{PL})^2}\frac{\partial \mathrm{p}}{\partial \mathrm{t}} \qquad (4.5)$$

Thus, equating the mass of free gas,

$$\frac{\partial}{\partial t}\left(\rho_g\phi_m + \rho_g V_{ads} * \rho_s\right) = \frac{\partial}{\partial t}\left(\frac{p_m M}{zRT}\phi_m\right) + \frac{\rho_s M}{V_{std}} * VL * \mathrm{PL} * \frac{1}{(p_m+\mathrm{PL})^2}\frac{\partial p_m}{\partial \mathrm{t}}$$

$$\frac{\partial}{\partial t}\left(\rho_g\phi_m + \rho_g V_{ads} * \rho_s\right) = \frac{M}{zRT}\phi_m * \frac{\partial p_m}{\partial t} + \frac{\rho_s M}{V_{std}} * VL * \mathrm{PL} * \frac{1}{(p_m+\mathrm{PL})^2}\frac{\partial p_m}{\partial \mathrm{t}}$$

$$\frac{\partial}{\partial t}\left(\rho_g\phi_m + \rho_g V_{ads} * \rho_s\right) = \frac{\partial p_m}{\partial t}\left(\frac{M}{zRT}\phi_m + \frac{\rho_s M}{V_{std}} * VL * \mathrm{PL} * \frac{1}{(p_m+\mathrm{PL})^2}\right) = \frac{\partial(\phi\rho)}{\partial t}$$

Considering the assumption of the matrix in 2D and the coordination equation

$$\nabla.\rho\mathbf{v} = \frac{\partial}{\partial x}\left(\rho_g v_x\right) + \frac{\partial}{\partial y}\left(\rho_g v_y\right)$$

Darcy's law is employed to represent the velocity flow within the matrix (Shen, Li, Xu, & Sun, 2017)

i.e.,

$$\boldsymbol{v} = -\frac{1}{\mu}\boldsymbol{K}.(\nabla p)$$

The x direction =

$$v_{\boldsymbol{x}} = -\frac{k_x}{\mu_g}\left(\frac{\partial p_m}{\partial \mathrm{x}}\right)$$

The y direction=

$$v_{\boldsymbol{y}} = -\frac{k_y}{\mu_g}\left(\frac{\partial p_m}{\partial \mathrm{y}}\right)$$

Thus

$$\nabla.\rho\mathbf{v} = \frac{\partial}{\partial x}\left(\rho_g * -\frac{k_x}{\mu_g}\left(\frac{\partial p_m}{\partial \mathrm{x}}\right)\right) + \frac{\partial}{\partial y}\left(\rho_g * -\frac{k_y}{\mu_g}\left(\frac{\partial p_m}{\partial \mathrm{y}}\right)\right) \qquad (4.6)$$

From the continuity equation

$$\frac{\partial(\phi\rho)}{\partial t} = -\nabla.\rho\mathbf{v}$$

Considering the flow system in the shale layer as gas is transported from the matrix to the natural fractures, hence it is described by

$$\frac{\partial(\phi\rho)}{\partial t} = -\nabla.\rho\mathbf{v} - q_m \qquad (4.7)$$

where q_m = the interporosity flow model in form of diffusion (kg/m^3.s)

With the use of Darcy's law;

$$q_m = \frac{\rho_g k_{ma} \alpha_{m \to NF} (p_m - p_{NF})}{\mu_g} \qquad (4.8)$$

substituting equation (4.4), (4.6), (4.8) into (4.7)

$$\frac{\partial p_m}{\partial t}\left(\frac{M}{zRT}\phi_m + \frac{\rho_s M}{V_{std}} * VL * \mathrm{PL} * \frac{1}{(\mathrm{p_m} + \mathrm{PL})^2}\right) = -\left[\frac{\partial}{\partial x}\left(\rho_g * -\frac{k_{ma}}{\mu_g}\left(\frac{\partial p_m}{\partial \mathrm{x}}\right)\right) + \frac{\partial}{\partial y}\left(\rho_g * -\frac{k_{ma}}{\mu_g}\left(\frac{\partial p_m}{\partial \mathrm{y}}\right)\right)\right] - \left[\frac{\rho_g k_{ma} \alpha_{m \to NF} (p_m - p_{NF})}{\mu_g}\right]$$

simplified to

$$\frac{\partial p_m}{\partial t}\left(\frac{M}{zRT}\phi_m + \frac{\rho_s M}{V_{std}} * VL * \mathrm{PL} * \frac{1}{(\mathrm{p_m} + \mathrm{PL})^2}\right) = \frac{\rho_g k_{ma}}{\mu_g} * \frac{\partial^2 \mathrm{p_m}}{\partial x^2} + \frac{\rho_g k_{ma}}{\mu_g} * \frac{\partial^2 \mathrm{p_m}}{\partial y^2} - \left[\frac{\rho_g k_{ma} \alpha_{m \to NF} (p_m - p_{NF})}{\mu_g}\right]$$

dividing through with the gas constant;

$$\frac{\partial p_m}{\partial t}\left(\phi_m + \frac{\rho_s * RT}{V_{std}} * VL * \mathrm{PL} * \frac{1}{(\mathrm{p_m} + \mathrm{PL})^2}\right) = \frac{k_{ma}}{\mu_g} * \frac{\partial^2 \mathrm{p_m}}{\partial x^2} + \frac{k_{ma}}{\mu_g} * \frac{\partial^2 \mathrm{p_m}}{\partial y^2} - \left[\frac{k_{ma} \alpha_{m \to NF} (p_m - p_{NF})}{\mu_g}\right]$$

(6)

Where,

μ_g= the gas viscosity

K_{ma} = matrix apparent permeability

$\alpha_{m\to NF}$ = the interporosity shape factor from the matrix to the natural fractures

To determine the final equation, parameters from table x & y are inserted into equation (6) to give;

$$0.05\frac{\partial p_m}{\partial t} = 3.952\times10^{-10}\frac{\partial^2 p_m}{\partial x^2} + 3.952\times10^{-10}\frac{\partial^2 p_m}{\partial y^2} - 1.984\times10^{-9}(20\times10^6 - p_{NF})$$

(4.9)

Initial boundary: $p_m = p_i,\ t = 0$

Boundary condition: $\frac{\partial p_m}{\partial n}_{\Gamma} = 0,\ t > 0$

4.3 The flow equation of the natural fractures

In this phase only free gas exists, hence the rate of mass accumulation is expressed as;

$$\frac{\partial}{\partial t}(\phi_{NF}.\rho_g)$$

Taking into account the two-dimensional coordination equation and the continuity equation;

$$\frac{\partial(\phi\rho)}{\partial t} = -\nabla.\rho\mathbf{v}$$

$$\frac{\partial}{\partial t}(\phi_{NF}.\rho_g) = -\left[\frac{\partial}{\partial x}(\rho_g v_x) + \frac{\partial}{\partial y}(\rho_g v_y)\right] + q_m - q_f$$

q_f = the flow term from the natural fractures to the hydraulic fractures

$$q_f = \frac{\rho_g k_{NFa} \alpha_{NF\to HF}(p_{NF} - p_{HF})}{\mu_g} \qquad (4.10)$$

$\alpha_{NF\to HF}$ represents the interporosity flow from the natural fractures to hydraulic fractures.

Due to the flow of the natural fractures existing in form of Darcy flow, the permeability shall not be altered. Thus, the continuity equation in the natural fracture is expressed as

$$\frac{\partial}{\partial t}\left(\phi_{NF}.\frac{p_{NF}M}{zRT}\right) = \frac{\rho_g k_{NF}}{\mu_g} * \frac{\partial^2 \mathrm{p_{NF}}}{\partial x^2} + \frac{\rho_g k_{NF}}{\mu_g} * \frac{\partial^2 \mathrm{p_{NF}}}{\partial y^2} + \frac{\rho_g k_{ma} \alpha_{m\to NF}(p_m - p_{NF})}{\mu_g} - \frac{\rho_g k_{NF} \alpha_{NF\to HF}(p_{NF} - p_{HF})}{\mu_g}$$

after factorizing the constants;

$$\frac{\phi_{NF}M}{zRT}.\frac{\partial p_{NF}}{\partial t} = \frac{\rho_g k_{NF}}{\mu_g} * \frac{\partial^2 \mathrm{p_{NF}}}{\partial x^2} + \frac{\rho_g k_{NF}}{\mu_g} * \frac{\partial^2 \mathrm{p_{NF}}}{\partial y^2} + \frac{\rho_g k_{ma} \alpha_{m\to NF}(p_m - p_{NF})}{\mu_g} - \frac{\rho_g k_{NF} \alpha_{NF\to HF}(p_{NF} - p_{HF})}{\mu_g} \qquad (4.11)$$

Diving through with the gas density constant;

$$\frac{\phi_{NF}}{p_{NF}}.\frac{\partial p_{NF}}{\partial t} = \frac{k_{NF}}{\mu_g} * \frac{\partial^2 \mathrm{p_{NF}}}{\partial x^2} + \frac{k_{NF}}{\mu_g} * \frac{\partial^2 \mathrm{p_{NF}}}{\partial y^2} + \frac{k_{ma} \alpha_{m\to NF}(p_m - p_{NF})}{\mu_g} - \frac{k_{NF} \alpha_{NF\to HF}(p_{NF} - p_{HF})}{\mu_g} \qquad (4.12)$$

Again, inserting values from table X & Y to obtain the final equation,

$$0.01\frac{\partial p_{NF}}{\partial t} = 7.80 \times 10^{-5}\frac{\partial^2 p_{NF}}{\partial x^2} + 7.80 \times 10^{-5}\frac{\partial^2 p_{NF}}{\partial y^2} + 1.976 \times 10^{-15}(20 \times 10^6 - p_{NF}) - 1.976 \times 10^{-9}(20 \times 10^6 - p_{HF}) \qquad (4.13)$$

Initial boundary: $p_{NF} = p_i,\ t = 0$

Boundary condition: $\frac{\partial p_{NF}}{\partial n}_{\Gamma} = 0,\ t > 0$

4.4 The flow equation of the hydraulic fractures

In the same manner as the natural fractures, flow within the hydraulic fractures is considered as Darcy flow and the permeability is also not altered in developing the equation. We also assume that the flow is one dimensional (1D), thus the continuity equation is written as,

$$\frac{\partial}{\partial t}(\phi_{HF}.\rho_g) = -\left[\frac{\partial}{\partial y}(\rho_g v_y)\right] + q_f - q_w \qquad (4.14)$$

q_w symbolizes the flow system from the hydraulic fractures to the horizontal well which is represented as,

$$q_w = \frac{2\pi\rho_g k_{HF}(p_{HF}-p_w)}{\Delta x\Delta y\mu_g \ln\left(\frac{r_e}{r_w}\right)} \qquad (4.15)$$

$$r_e = 0.14\sqrt{\Delta x^2 + \Delta y^2}$$

Δx and Δy is where the grid of the hydraulic fracture intersects the horizontal well (Zhang, et al., 2017).

Substituting q_w into equation (4.14), the continuity equation

$$\frac{\phi_{HF}M}{zRT}.\frac{\partial p_{HF}}{\partial t} = \frac{\rho_g k_{HF}}{\mu_g} * \frac{\partial^2 \mathrm{p_{HF}}}{\partial y^2} + \frac{\rho_g k_{NF}\alpha_{NF\to HF}(p_{NF}-p_{HF})}{\mu_g} - \frac{2\pi\rho_g k_{HF}(p_{HF}-p_w)}{\Delta x\Delta y\mu_g \ln\left(\frac{r_e}{r_w}\right)}$$

Once again dividing through by the constant gas density to give;

$$\frac{\phi_{HF}}{p_{HF}}.\frac{\partial p_{HF}}{\partial t} = \frac{k_{HF}}{\mu_g} * \frac{\partial^2 \mathrm{p_{HF}}}{\partial y^2} + \frac{k_{NF}\alpha_{NF\to HF}(p_{NF}-p_{HF})}{\mu_g} - \frac{2\pi k_{HF}(p_{HF}-p_w)}{\Delta x\Delta y\mu_g \ln\left(\frac{r_e}{r_w}\right)} \qquad (4.16)$$

After inserting the known parameters into the equation above, the final equation becomes;

$$\frac{\partial p_{HF}}{\partial t} = 6.241 \times 10^{-9} \frac{\partial^2 p_{HF}}{\partial y^2} + 3.897 \times 10^{-12}(20 \times 10^6 - p_{HF}) - 6.44 \times 10^{-7} \qquad (4.17)$$

Initial boundary: $p_{HF} = p_i,\ t = 0$

Outer boundary condition: $\frac{\partial p_m}{\partial n}_{\Gamma} = 0;\ t > 0$

Inner boundary condition: $q_w = \frac{2\pi\rho_g k_{HF}(p_{HF} - p_w)}{\Delta x \Delta y \mu_g \ln\left(\frac{r_e}{r_w}\right)};\ t > 0$

Chapter 5 METHODS USED IN SOLVING FLOW EQUATION

After developing the continuity equations of the three medias and inserting parameters derived from field data, the differential equations are solved considering its boundary conditions to determine the mass of gas in each media. Some studies have derived a triple porosity model analytically, however the analytical method has been found not capable of solving the flow model equations. Hence, the numerical method is suggested when solving the governing equations. Finite Difference Method (FDM) and Finite Element Method (FEM) are the most common and well-developed methods used while solving equations numerically (Zhang et al, 2019).

5.1 Finite Difference Method

This method is regarded as an easy and well-developed method used in solving differential equations (Bui, 2009). It is proposed for reservoir simulation and an even larger scale of flow simulation. This method involves the discretization of ordinary or partial differential equations in order to model the reservoir flow (Zhang et al, 2019). The partial differential equations are solved numerically at predefined set of discrete points, known as nodal points in the structured grid, starting by identifying the grid points of the given domain, which is the first step in the finite difference approximation called discretization of the domain. The discrete points are then uniformly inserted and connected by straight lines which gives the required grid, and the controlled partial equations are approximated or discretized at the identified grid points. Afterwards, the algebraic equations obtained by approximation or discretization are solved using direct or iterative methods; here the iterative method is used to approximate the derivatives in finite differences. The accuracy of the results obtained through the finite difference method has been found to be accurate

and greatly relevant to the block divisions and boundary conditions (Shabro, Torres-Verdin et al, 2012).

5.2 Finite Element Method

The finite element method is more accurate and mostly recommended for reservoir simulation compared to the finite different method. It is a numerical method which accommodates the flexibility of unstructured meshes, because of this, the FEM is more suitable in describing the flow properties and complexities in a less permeable reservoir from the fractures to the matrix systems effectively and efficiently (Jayakumar, Sahai and Boulis, 2011). The method provides a systematic approach to piecewise approximation over subdomains that produces sequences of functions that can approximate arbitrarily closely in appropriate norms. This attribute is referred to as a property of "interpolation" for FEMs. It basically lifts the idea of approximate function representation from the classical notion of interpolation across values of functions or values of derivatives to a general approach for approximating functions with generalized derivatives (Oden, 2010).

5.3 Solution to Developed Model

The derived numerical flow equations are solved through the Finite Difference Method. Equation (4.9), (4.13) as well as (4.17) are in a partial differential equation form and will be solved to get the algorithm to be applied on MATLAB. Equation (4.17) is first solved to find p_{HF} which is then substituted into (4.13) to find p_{NF} and lastly, both values of p_{HF} and $p_{NF}$are substituted into (4.9) to find p_m.

5.3.1 Hydraulic Fracture Phase

$$\frac{\partial p_{HF}}{\partial t} = 6.241 \times 10^{-9} \frac{\partial^2 p_{HF}}{\partial y^2} + 3.897 \times 10^{-12}(20 \times 10^6 - p_{HF}) - 6.44 \times 10^{-7} \quad (5.1)$$

Initial boundary: $p_{HF} = p_i = 20 \times 10^6\ Pa, y = 0,\ t \geq 0$

Outer boundary condition: $\frac{\partial p_m}{\partial n}_{\Gamma} = 0;\ t > 0$

Inner boundary condition: $p_{HF} = p_w = 5 \times 10^6\ Pa,\ t > 0$

Equation (5.1) is of the general diffusion equation in one dimension and is represented as;

$$\frac{\partial p}{\partial t} = b \frac{\partial^2 p}{\partial y^2} + F(y, t)$$

- Where; p (y, t): the unknown function we want to find
- b: known constant
- F (y, t): known pressure source distribution

Derivatives are approximated using finite difference method:

$$\frac{\partial p}{\partial t} \approx \frac{p_i^{k+1} - p_i^k}{\Delta t}$$

$$\frac{\partial^2 p}{\partial y^2} \approx \frac{p_{i-1}^k - 2p_i^k + p_{i+1}^k}{\Delta y^2}$$

Therefore, the approximation of the hydraulic fracture using finite difference method is:

$$\frac{p_i^{k+1} - p_i^k}{\Delta t} = b\frac{p_{i-1}^k - 2p_i^k + p_{i+1}^k}{\Delta y^2} + F(y_i, t_k)$$

Explicit method:

$$p_i^{k+1} = p_i^k + b\frac{\Delta t}{\Delta y^2}\left(p_{i-1}^k - 2p_i^k + p_{i+1}^k\right) + \Delta t F(y_i, k); 0 < b\frac{\Delta t}{\Delta y^2} < 0.5$$

$$p_i^{k+1} = p_i^k + b\frac{\Delta t}{\Delta y^2}\left(p_{i-1}^k - 2p_i^k + p_{i+1}^k\right) + \Delta t\left[6.241 \times 10^{-9}\left(20 \times 10^6 - p_i^b\right) - 6.44 \times 10^{-7}\right]$$

5.3.2 Natural Fracture Phase

$$0.01\frac{\partial p_{NF}}{\partial t} = 7.80 \times 10^{-5}\frac{\partial^2 p_{NF}}{\partial x^2} + 7.80 \times 10^{-5}\frac{\partial^2 p_{NF}}{\partial y^2} + 1.976 \times 10^{-15}(20 \times 10^6 - p_{NF}) -$$

$$1.976 \times 10^{-9}(20 \times 10^6 - p_{HF}) \qquad (5.2)$$

Initial boundary: $p_{NF} = p_i = 20 \times 10^6\ Pa,\ t = 0$

Outer boundary condition: $p_{NF} = p_i = 20 \times 10^6\ Pa$

$$\frac{\partial p_{NF}}{\partial n}_{\Gamma} = 0, \qquad t > 0$$

Inner boundary condition: $p_{NF} = p_w = 5 \times 10^6\ Pa$

Considering the general diffusion equation in two dimension (2D), it is therefore represented as;

$$\frac{\partial p(y,t)}{\partial t} = c\left(\frac{\partial^2 p}{\partial x^2} + \frac{\partial^2 p}{\partial y^2}\right) + F(p, x, y)$$

The differential equation derivates are approximated just as in the hydraulic fracture phase

$$\frac{\partial p}{\partial t} \approx \frac{p_i^{l+1} - p_i^l}{\Delta t}$$

$$\frac{\partial^2 p}{\partial x^2} \approx \frac{p_{i+1}^l - 2p_i^l - p_{i-1}^l}{\Delta x^2}$$

$$\frac{\partial^2 p}{\partial y^2} \approx \frac{p_{i+1}^l - 2p_i^l - p_{i-1}^l}{\Delta y^2}$$

Therefore, the approximation of the natural fracture using finite difference method is:

$$\frac{p_{i,j}^{l+1} - p_{i,j}^l}{\Delta t} = b\left(\frac{p_{i,j+1}^l - 2p_i^l + p_{i,j-1}^l}{\Delta x^2} + \frac{p_{i,j+1}^l - 2p_{i,j}^l + p_{i,j-1}^l}{\Delta y^2}\right) + F(p_{k,l}, x_{i,j}, y_{i,j})$$

Explicitly

$$p_{i,j}^{l+1} = p_{i,j}^l + b\frac{\Delta t}{\Delta x^2}\left(p_{i,j+1}^l - 2p_{i,j}^l + p_{i,j-1}^l\right) + c\frac{\Delta t}{\Delta y^2}\left(p_{i,j+1}^l - 2p_{i,j}^l + p_{i,j-1}^l\right)$$
$$+ \Delta t\left[1.976 \times 10^{-15}\left(20 \times 10^6 - p_{i,j}^l\right) - 1.976 \times 10^{-9}\left(20 \times 10^6 - p_i^k\right)\right]$$

5.3.3 Matrix Phase

$$0.05\frac{\partial p_m}{\partial t} = 3.952 \times 10^{-10}\frac{\partial^2 p_m}{\partial x^2} + 3.952 \times 10^{-10}\frac{\partial^2 p_m}{\partial y^2} - 1.984 \times 10^{-9}(20 \times 10^6 - p_{NF})$$

(5.3)

Initial boundary: $p_m = p_i = 20 \times 10^6\ Pa,\ t = 0$

Outer boundary condition: $p_m = p_i = 20 \times 10^6\ Pa$

$$\frac{\partial p_m}{\partial n}_{\Gamma} = 0, \qquad t > 0$$

Inner boundary condition: $p_m = p_w = 5 \times 10^6\ Pa$

In the same form as the natural fractures, the matrix phase general diffusion equation is in 2D and follows the same approximation to obtain its derivates. Therefore, the approximation of the matrix phase using finite difference method is:

$$p_{i,j}^{n+1} = p_{i,j}^{n} + b\frac{\Delta t}{\Delta x^2}\left(p_{i,j-1}^{n} - 2p_{i,j}^{n} + p_{i,j+1}^{n}\right) + b\frac{\Delta t}{\Delta y^2}\left(p_{j,i-1}^{n} - 2p_{i,j}^{n} + p_{i,j+1}^{n}\right)$$
$$+ \Delta t\left[1.984 \times 10^{-9}(20 \times 10^6 - p_{i,j}^{m})\right]$$

Chapter 6 RESULTS & DISCUSSION

Once the partial differential equations of the matrix phase, natural fractures and hydraulic fractures were solved using the Finite Difference Method by discretizing the equations in each medium to its final form with its initial and boundary conditions, a code was developed to illustrate the reservoir pressure distribution with respect to time. The graphs below will describe the pressure increase at different points in the reservoir before the gas is released and then declines, thus affecting the total gas production rate.

6.1 Matrix Phase

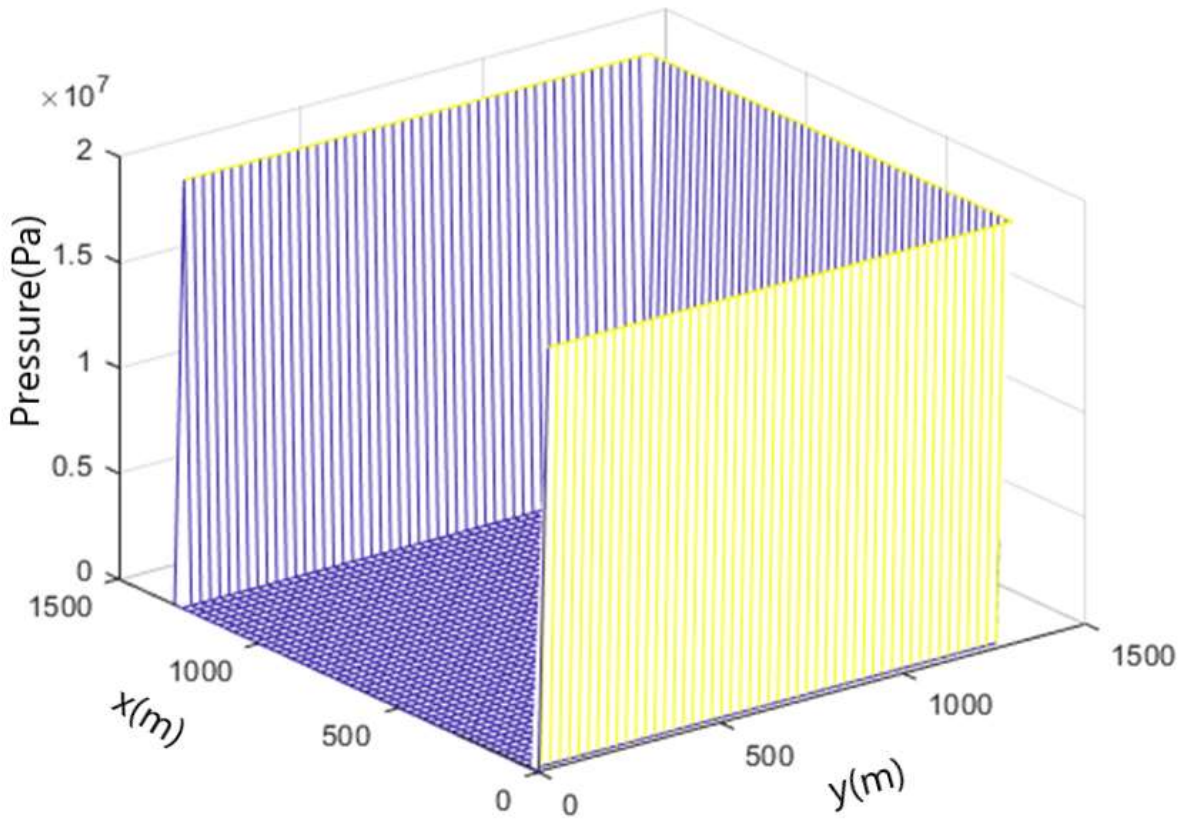


Figure 6.1 Reservoir pressure distribution in the matrix phase against time.

The pressure distribution in Figure 6.1 demonstrates natural properties as a result of the presence of the original gas which is absorbed inside the surface of the matrix pores. The transient pressure of most of the diffused gas exists in its original state and the graph is modeled in a grid block model in an X, Y and Z direction, the matrix blocks stimulates nearby fractures and transports fluids to well location through the fractures (Cai, 2014). Due to the low permeability in the matrixes, a lot of pore volume exists in the reservoir with very few contributions to the flow, hence the matrix poses no effect on the total gas production. This behavior is as a result of the properties of the reservoir with ultra-low permeability existing in a typical shale gas reservoir where adsorbed gas and gas diffusion processes co-exist in the matrixes.

6.2 Natural Fractures

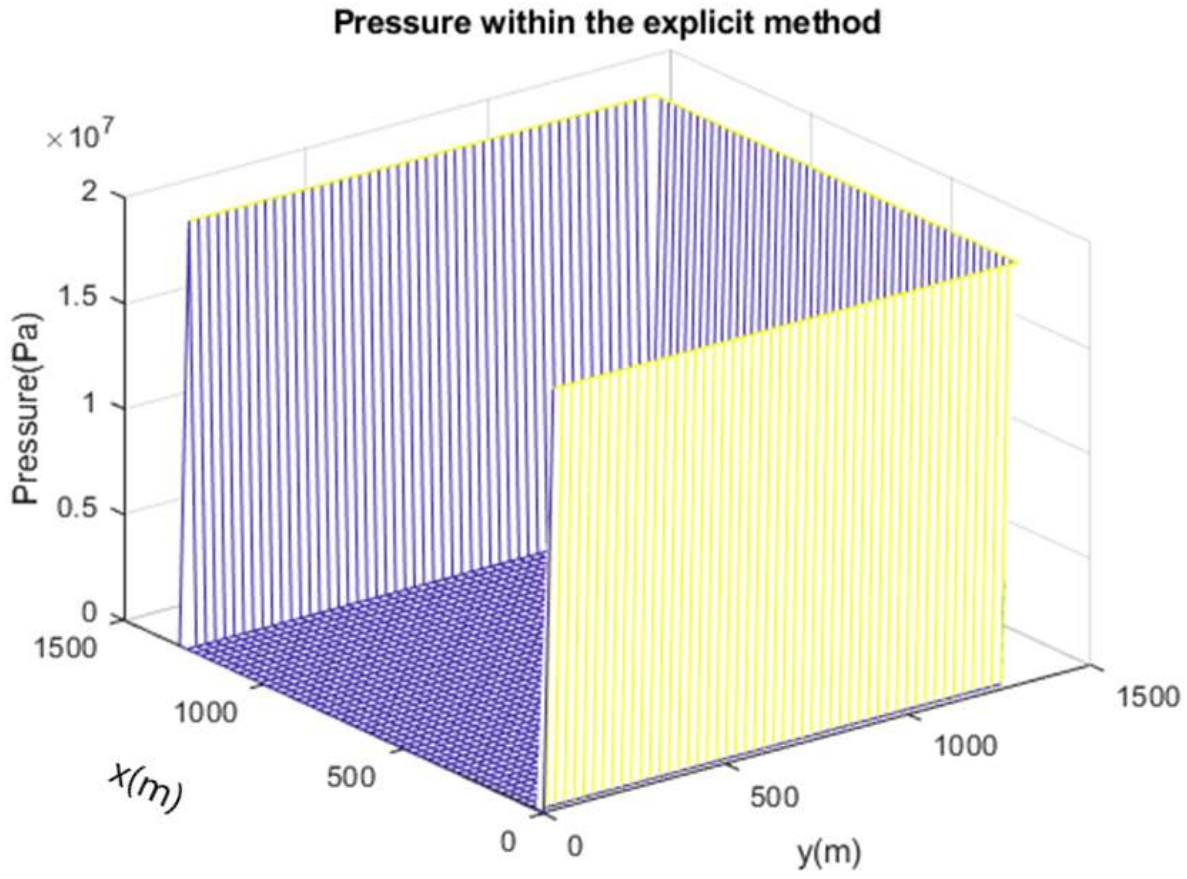


Figure 6.2 Reservoir pressure distribution in the natural fractures against time with u (1,j,k) =300x(k<120)+70

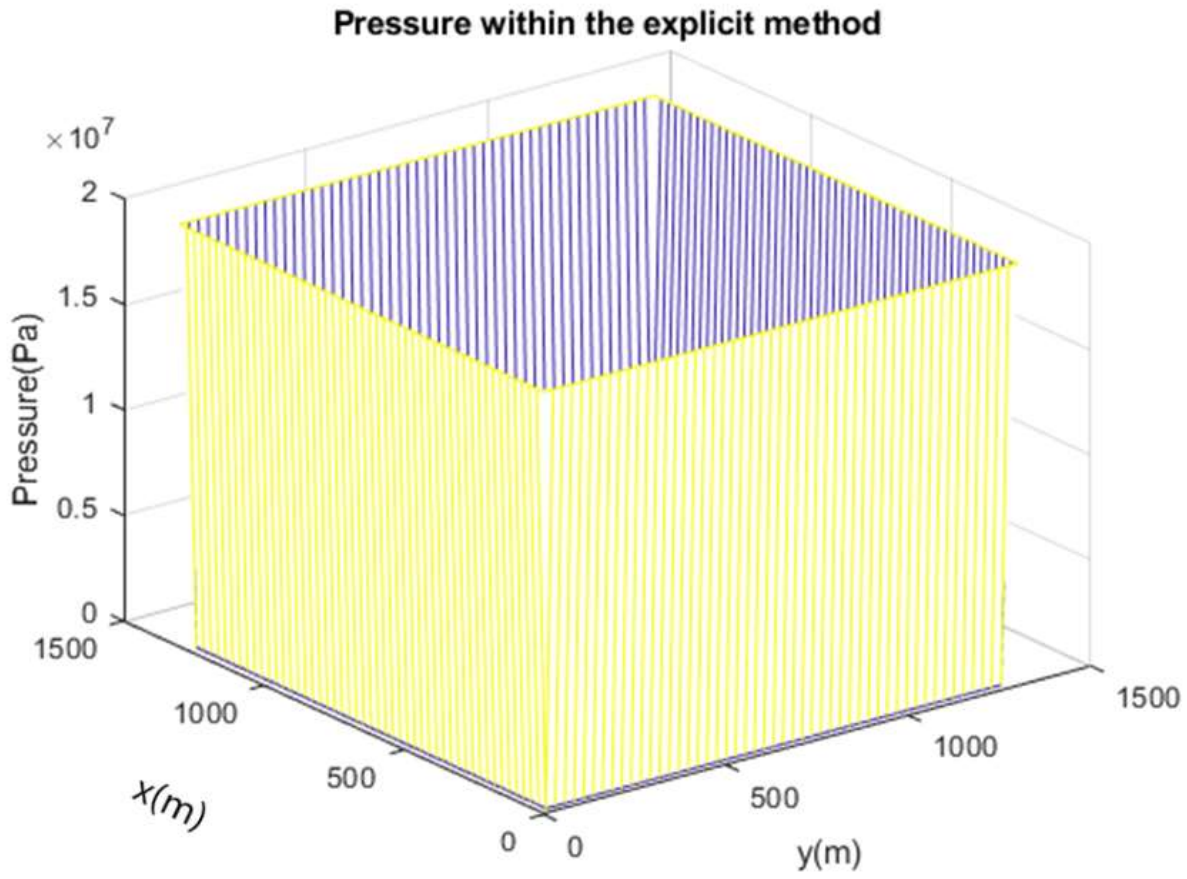


Figure 6.3 Reservoir pressure distribution in the natural fractures against time without u (1,j,k) =300x(k<120)+70

The behavior seen in Figures 6. 2 and 6.3 shows a pressure distribution within a matrix, in which the fluid flows in one direction between two defined boundaries with a progressive decrease in pressure. Furthermore, the difference in view between the two graphs shows that Fig 6.2 exists in a semi-closed grid block whereas Figure 6.3 exists in a closed grid block, demonstrating that the results indicate an obvious difference. In both Figures, the pressure declines slower in the early stages of production due to the gas compressibility factor and gas viscosity over a period of time, which matches the suggested model by Zhang, et al., (2017). It should be noted that the scheme displayed is a combined module in which each grid block interconnects with each other within the

connected network. Figure 6.3 displays the results of the pressure of the flow in the grid once effective permeability is eliminated, indicating that this factor affects the total cumulative production. This case without the effective permeability factor displays a slower flow of fluid and transient flow changes with production. The pressure profiles are similar to the matrix phase as a result of the gas transport in its natural state due to the rock properties that exists within the shale layer, however, the flow may be subject to changes dependent on the pressure gradient.

6.3 Hydraulic Fractures

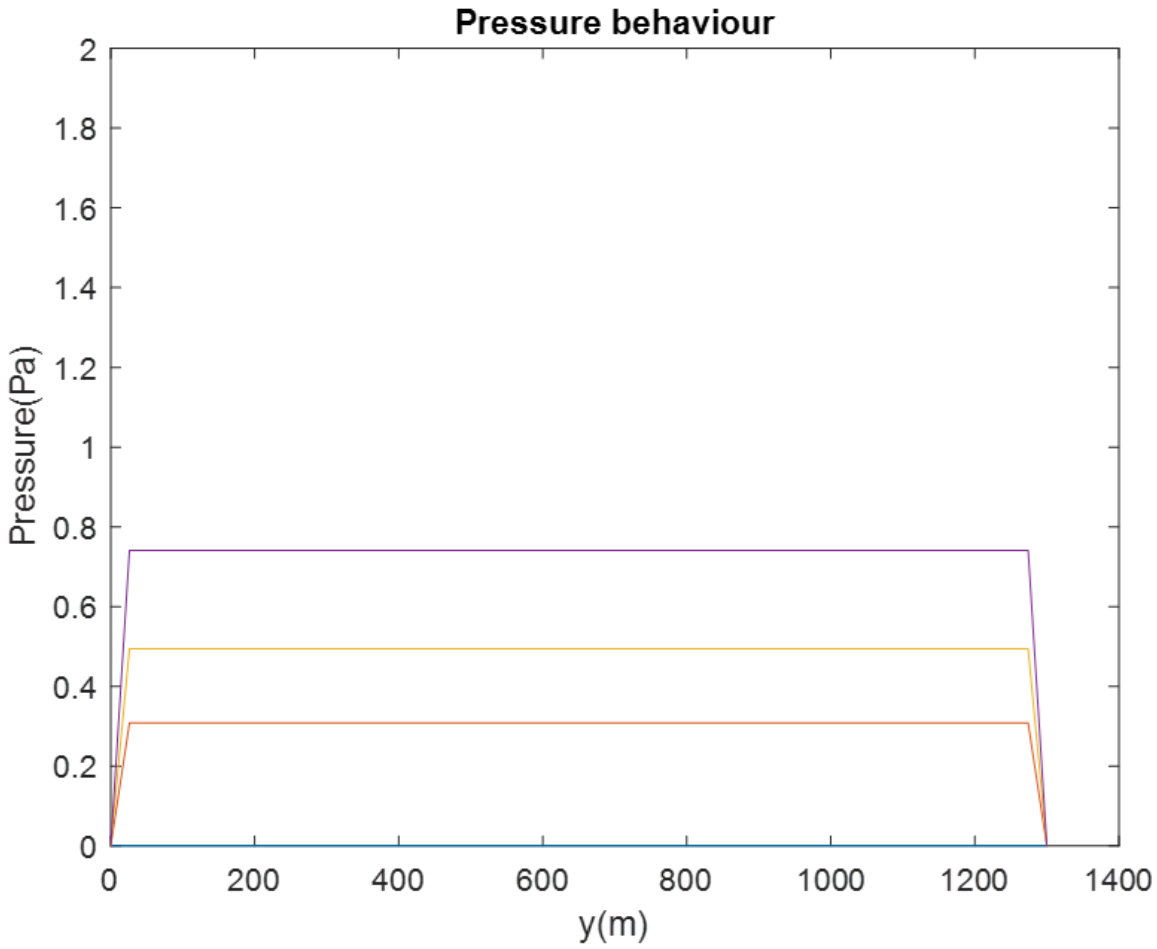


Figure 6.4 Reservoir pressure distribution in the hydraulic fractures against time

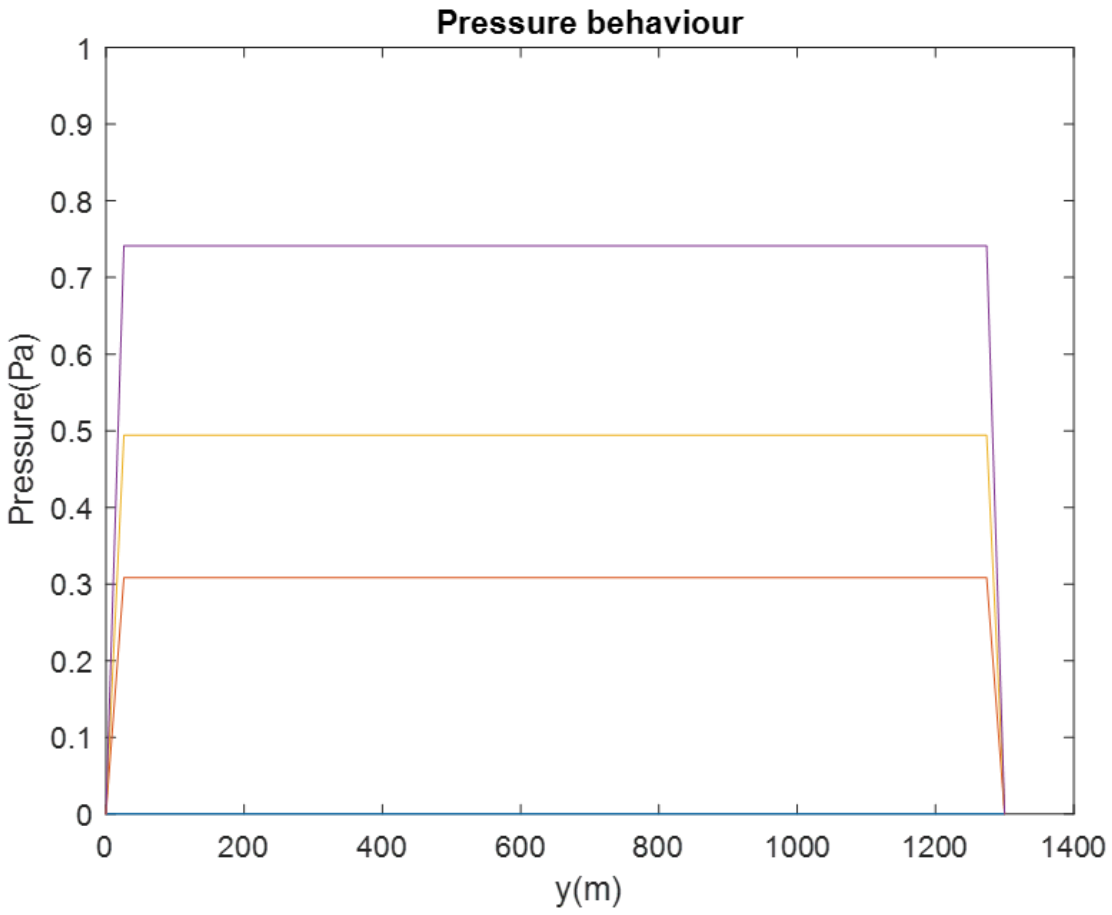


Figure 6.5 Reservoir pressure distribution in the hydraulic fractures against time

Figures 6.4 and 6.5 show that the pressure behavior in the hydraulic fracture remains constant over a period of time before the pressure drops which illustrates the flow of adsorbed gas into the reservoir with the known constant, b and agrees with the model proposed by Alhamadi (2010), whose simulation showed that the pressure decreases when the reservoir gets to its boundaries and once the reservoir boundaries are reached average reservoir pressure starts to decline. However, four other constant values were assumed to show the flow of adsorbed gas at different pressures.

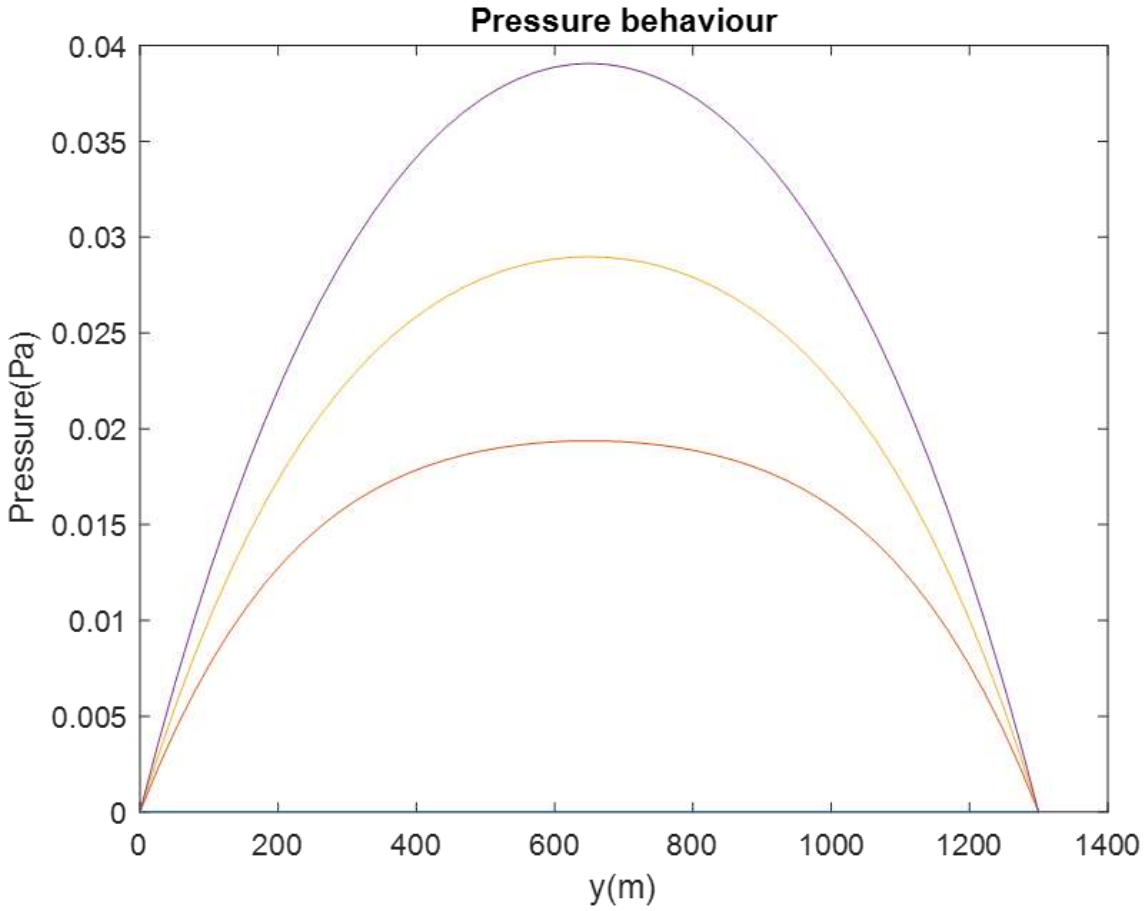


Figure 6.6 Pressure behavior in the hydraulic fractures against time, where the constant b is 0.18.

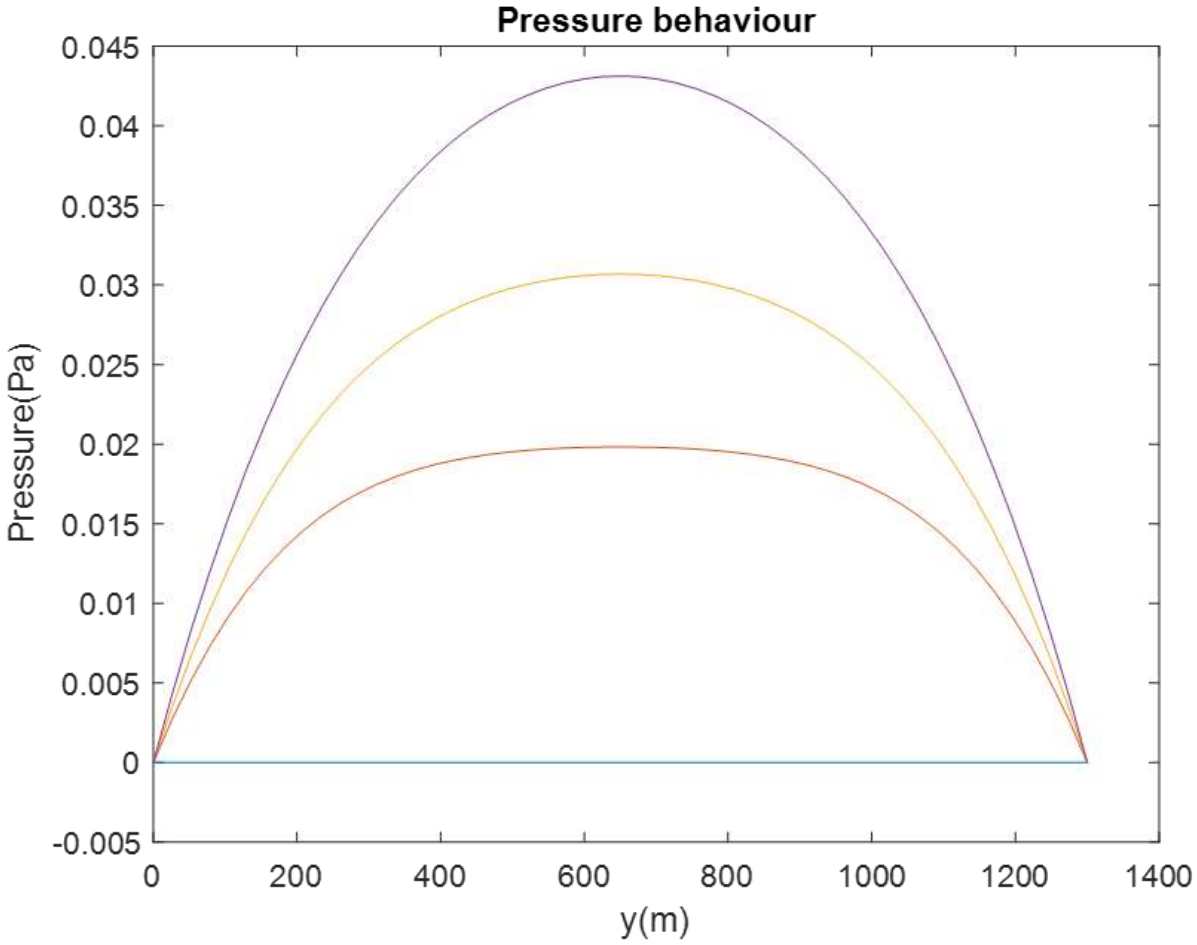


Figure 6.7 Pressure behavior in the hydraulic fractures against time, where the constant b is 0.13.

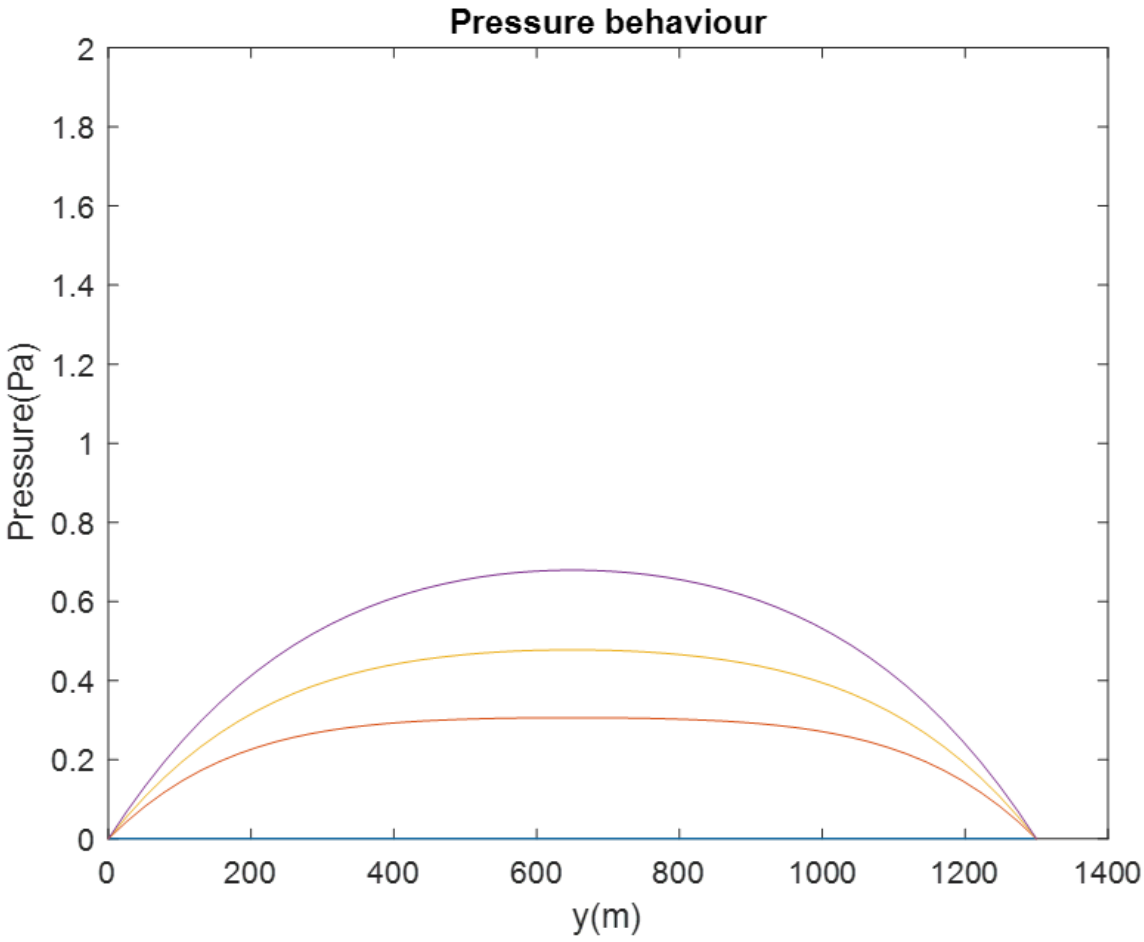


Figure 6.8 Pressure behavior in the hydraulic fractures against time, where the constant b is 0.11.

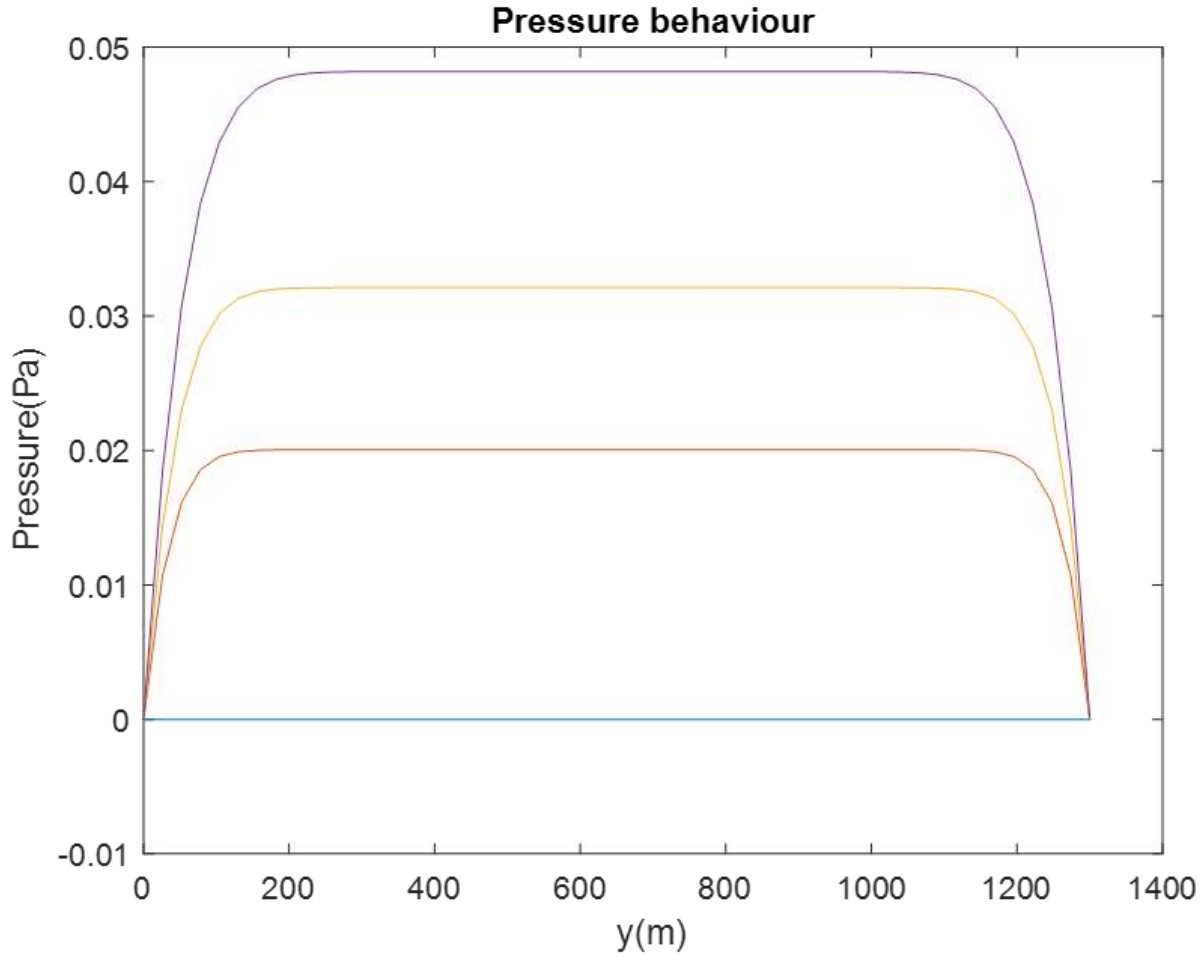


Figure 6.9 Pressure behavior in the hydraulic fractures against time, where the constant b is 0.05.

By increasing the known constants, Figure 6.9 shows the pressure dropping at a less abrupt rate compared to at a lower coefficient, this behavior matches the model estimated by Huang et al. (2015), where there was a slow drop in the reservoir pressure when the well was producing at a steady frequency. This shows a high gas production rate as the well is being produced under a constant wellbore pressure. Figures 6.8, 6.7, and 6.6 continue to exhibit similar pressure behaviors, indicating that the bigger the coefficient the less time it takes for the pressure of the adsorbed gas to drop in the reservoir thereby releasing the adsorbed gas in small volumes. This behavior once again confirms the numerical model estimated by Zhang, et al. (2017). The distribution of fractures

displayed in the graph shows that with a rise in pressure, the number of years the reservoir keeps producing gas drops. This means that after hydraulic fracturing, adsorbed gas will only be released over a period of time before reservoir pressure drops. Additionally, the pressure gradient slope behavior shows a series of build-ups where three pressure segments appear which represents the intensity of change at an early time, during the transition period and at late time which resembles a homogenous reservoir case as presented by Abdassah and Ershaghi, 1986. Their study confirms the analysis carried out in this research where reservoir pressure drawdown or pressure buildup affects the flow of gas in a shale reservoir.

From the graphs, the model shows deviations in the total produced gas as well as the reservoir pressure overtime; this behavior matches the model proposed by Zhang et al., (2015) where they looked at two possible alternatives to examine the reservoir permeability. They gave two reasons for these outcomes; firstly, as a result of the resistance in bulk inversion of the matrix system and secondly, due to more rapid reservoir pressure decrease in the dual porosity system compared to the triple porosity system. Furthermore, their model was concluded to give a high gas recovery rate and does not underestimate the total shale gas reservoir recovery.

Chapter 7 CONCLUSION

This study involved the development of a triple continuum model consisting of the matrix phase, natural fractures and hydraulic fractures. Three flow equations were developed and solved to demonstrate the behavior of gas and then modelled to predict the overall production of gas in a shale reservoir. The model was simulated using MATLAB and although the Karoo Basin in South Africa lacked sufficient data, the final results shown were verified using field data from already existing reservoir and upon analysis turned out to be in agreement with existing models. Therefore, this proves the accuracy of the developed model in this research and renders it viable for use in any reservoir.

From the analysis of results, the impact of flow characteristics take effect in the final production of gas in a shale reservoir and the rate of gas production is dependent on the pressure distribution in the reservoir. The fractures have similar components which are constant and interrelate with other arrays of separate matrixes which exhibit different permeabilities and porosities. According to the simulation derived from this research report, the reservoir permeability is the most significant factor with regards to production rate. The impact of the permeability existing in the natural and hydraulic fracture phases poses an effect on the pressure distribution within the shale reservoir. In the large permeability region gas production is more efficient, although a boundary needs to be established between a smaller permeability region and larger permeability region in other for shale gas exploitation to be possible. It is also acclaimed that the effect of dissolved gas in organic materials should be regarded in shale gas reservoir models.

Furthermore, a sensitivity analysis is recommended in order to assess the accuracy of the proposed model.

REFERENCES

Abanda, P.A. and Hannigan, R.E., 2006. Effect of diagenesis on trace element partitioning in shales. *Chemical Geology*, *230*(1-2), pp.42-59.

Aguilera, R.F. and Radetzki, M., 2014. The shale revolution: Global gas and oil markets under transformation. *Mineral Economics*, *26*(3), pp.75-84.

Al-Ahmadi, H.A., Almarzooq, A.M. and Wattenbarger, R.A., 2010, February. Application of linear flow analysis to shale gas wells—Field cases. In *SPE unconventional gas conference*. OnePetro.

Berawala, D.S., 2015. *Modelling of gas production from tight shale formations: An innovative approach* (Master's thesis, University of Stavanger, Norway).

Boyer, C., Clark, B., Jochen, V., Lewis, R. and Miller, C., 2011. Shale gas: A global resource, Oilfield Review. *Autum*, pp.28-31.

Bustin, A.M. and Bustin, R.M., 2012. Importance of rock properties on the producibility of gas shales. *International Journal of Coal Geology*, *103*, pp.132-147.

Cai, L., 2014. *Matrix-fracture interaction analysis in fractured unconventional gas reservoir*. Colorado School of Mines.

Chere, N., Linol, B., De Wit, M. and Schulz, H.M., 2017. Lateral and temporal variations of black shales across the southern Karoo Basin-Implications for shale gas exploration. *South African Journal of Geology 2017*, *120*(4), pp.541-564.

Cole, D.I., Robey, K., Chevallier, L. and Viljoen, J., 2011. The geology of shales with a gas potential in the Main Karoo Basin of South Africa and impact of hydraulic fracturing on groundwater. *Council for Geoscience Report*, *142*.

Conti, J., Holtberg, P., Diefenderfer, J., LaRose, A., Turnure, J.T. and Westfall, L., 2016. *International energy outlook 2016 with projections to 2040* (No. DOE/EIA-0484 (2016)). USDOE Energy Information Administration (EIA), Washington, DC (United States). Office of Energy Analysis.

Crossey, L.J., Loucks, R., Totten, M.W. and Scholle, P.A., 1996. Siliciclastic diagenesis and fluid flow: concepts and applications.

Curtis, J.B., 2002. Fractured shale-gas systems. *AAPG bulletin*, *86*(11), pp.1921-1938.

Dai, J., Zou, C., Liao, S., Dong, D., Ni, Y., Huang, J., Wu, W., Gong, D., Huang, S. and Hu, G., 2014. Geochemistry of the extremely high thermal maturity Longmaxi shale gas, southern Sichuan Basin. *Organic Geochemistry*, *74*, pp.3-12.

De Swaan O, A., 1976. Analytic solutions for determining naturally fractured reservoir properties by well testing. *Society of Petroleum Engineers Journal*, *16*(03), pp.117-122.

Gandossi, L. and Von Estorff, U., 2013. An overview of hydraulic fracturing and other formation stimulation technologies for shale gas production. *Eur. Commisison Jt. Res. Cent. Tech. Reports*, *26347*.

Geel, C., Schulz, H.M., Booth, P., deWit, M. and Horsfield, B., 2013. Shale gas characteristics of Permian black shales in South Africa: results from recent drilling in the Ecca Group (Eastern Cape). *Energy Procedia*, *40*, pp.256-265.

Guo, C., Wei, M. and Liu, H., 2015. Modeling of gas production from shale reservoirs considering multiple transport mechanisms. *PloS one*, *10*(12), p.e0143649.

Jiang, J. and Younis, R.M., 2015. A multimechanistic multicontinuum model for simulating shale gas reservoir with complex fractured system. *Fuel*, *161*, pp.333-344.

Kazemi, H., 1969. Pressure transient analysis of naturally fractured reservoirs with uniform fracture distribution. *Society of petroleum engineers Journal*, *9*(04), pp.451-462.

Langmuir, I., 1918. The adsorption of gases on plane surfaces of glass, mica and platinum. *Journal of the American Chemical society*, *40*(9), pp.1361-1403.

Lu, X.C., Li, F.C. and Watson, A.T., 1995. Adsorption studies of natural gas storage in Devonian shales. *SPE Formation evaluation*, *10*(02), pp.109-113.

Mair, R., Bickle, M., Goodman, D., Koppelman, B., Roberts, J., Selley, R., Shipton, Z., Thomas, H., Walker, A., Woods, E. and Younger, P., 2012. Shale gas extraction in the UK: a review of hydraulic fracturing.

McCarthy, T. and Rubidge, B., 2005. The story of Earth and Life A southern African perspective on a 4.6-billion year journey. published by Struik. *Cape Town*, p.333.

McGlade, C., Speirs, J. and Sorrell, S., 2013. Unconventional gas–a review of regional and global resource estimates. *Energy*, *55*, pp.571-584.

Operations, H.F. and Construction, W., 2009. Integrity Guidelines. *Report (HF1), American Petroleum Institute, Washington, DC*.

Ozkan, E., Ohaeri, U. and Raghavan, R., 1987. Unsteady flow to a well-produced at a constant pressure in a fractured reservoir. *SPE Formation Evaluation*, *2*(02), pp.186-200.

Suárez-Ruiz, I., Flores, D., Mendonça Filho, J.G. and Hackley, P.C., 2012. Review and update of the applications of organic petrology: Part 1, geological applications. *International Journal of Coal Geology, 99*, pp.54-112.

Swami, V., Clarkson, C.R. and Settari, A.T., 2012, October. Non-Darcy flow in shale nanopores: do we have a final answer?. In *SPE Canadian unconventional resources conference*. OnePetro.

Swana, K., 2016. *Application of hydrochemistry and residence time constraints to distinguish groundwater systems in the Karoo Basin prior to shale-gas exploration* (Doctoral dissertation, Stellenbosch: Stellenbosch University).

Tanaka, N., 2010. World energy outlook 2010. *International Energy Agency. Paris: IEA*.

Tian, L., Xiao, C., Liu, M., Gu, D., Song, G., Cao, H. and Li, X., 2014. Well testing model for multi-fractured horizontal well for shale gas reservoirs with consideration of dual diffusion in matrix. *Journal of Natural Gas Science and Engineering*, *21*, pp.283-295.

UNEP, 2011. Oil palm plantations: threats and opportunities for tropical ecosystems. *United Nations Environment Programme (UNEP), Global Environmental Alert Service (GEAS)*.

UNEP, 2011a. (2011) "Athabasca oil sands, require massive investments and energy and produce massive amounts of oil and CO2".

United States. Energy Information Administration and Kuuskraa, V., 2011. *World shale gas resources: an initial assessment of 14 regions outside the United States*. US Department of Energy.

United States. Environmental Protection Agency. Office of Research and Development, 2011. *Plan to study the potential impacts of hydraulic fracturing on drinking water resources*. Office of Research and Development, US Environmental Protection Agency.

US Energy Information Administration ed., 2011. *Annual Energy Outlook 2011: With Projections to 2035*. Government Printing Office.

Vengosh, A., Jackson, R.B., Warner, N., Darrah, T.H. and Kondash, A., 2014. A critical review of the risks to water resources from unconventional shale gas development and hydraulic fracturing in the United States. *Environmental science & technology*, *48*(15), pp.8334-8348.

Wang, F.P. and Reed, R.M., 2009, October. Pore networks and fluid flow in gas shales. In *SPE annual technical conference and exhibition*. OnePetro

Wang, H.T., 2014. Performance of multiple fractured horizontal wells in shale gas reservoirs with consideration of multiple mechanisms. *Journal of Hydrology*, *510*, pp.299-312.

Wang, J.G., Kabir, A., Liu, J. and Chen, Z., 2012. Effects of non-Darcy flow on the performance of coal seam gas wells. *International Journal of Coal Geology*, *93*, pp.62-74.

Warren, J.E. and Root, P.J., 1963. The behavior of naturally fractured reservoirs. *Society of Petroleum Engineers Journal*, *3*(03), pp.245-255.

Welte, D.H. and Tissot, P.B., 1984. *Petroleum formation and occurrence*. Springer-verlag.

Wilde, P., Lyons, T.W. and Quinby-Hunt, M.S., 2004. Organic carbon proxies in black shales: molybdenum. *Chemical Geology*, *206*(3-4), pp.167-176.

Xiphu, M.R., Mills, S.R., Chevallier, L., Marot, J., Mkhize, M., Motloung, T., Ngesi, P., Okonkwo, A., Msmart, M., Solomons, M. and Tiplady, A., 2012. Report on Inves-tigation of Hydraulic Fracturing in the Karoo Basin of South Africa. *Resources DoM*, *96*, p.70.

Yu, W. and Sepehrnoori, K., 2013, April. Simulation of gas desorption and geomechanics effects for unconventional gas reservoirs. In *SPE Western Regional & AAPG Pacific Section Meeting 2013 Joint Technical Conference*. OnePetro.

Zhang, W., Xu, J. and Jiang, R., 2017. Production forecast of fractured shale gas reservoir considering multi-scale gas flow. *Journal of Petroleum Exploration and Production Technology*, *7*(4), pp.1071-1083.

Zhang, W., Xu, J., Jiang, R., Cui, Y., Qiao, J., Kang, C. and Lu, Q., 2017. Employing a quad-porosity numerical model to analyze the productivity of shale gas reservoir. *Journal of Petroleum Science and Engineering*, *157*, pp.1046-1055.

Zhang, T., Sun, S. and Song, H., 2019. Flow mechanism and simulation approaches for shale gas reservoirs: A review. *Transport in Porous Media*, *126*(3), pp.655-681.

APPENDICES

Appendix A

```
clear;
L = 1300;    % length in the x-direction (m)
W = 600;     % length in the y-direction (m)
Tend = 1300.;% final time (Days)
maxk = 2500;
dt = Tend/maxk;
n = 50.;     % Number of space steps

%%%%%%%%%%%%%%%%%%%%%%%%%%%%%%%%%%%%%%%%%%%%%%%%%%%%%%%%%%%%%%%%%%%%%%%%%%%%%%%

% initial condition and part of boundary condition
u(1:n+1,1:n+1,1:maxk+1) = 20*10^6.;
dx = L/n;
dy = W/n;   % use dx = dy = h
h = dx;
b = dt/(h*h);
cond = 3.952*10^(-10);    % thermal conductivity
spheat = 1.0;   % specific heat
rho = 1.;   % density
a = cond/(spheat*rho);
alpha = a*b;
c = 7.8*10^(-5);
for i = 1:n+1
   x(i) =(i-1)*h;   % use dx = dy = h
   y(i) =(i-1)*h;
end
%%%%%%%%%%%%%%%%%%%%%%%%%%%%%%%%%%%%%%%%%%%%%%%%%%%%%%%%%%%%%%%%%%%%%%%%%%%%%%%

% boundary condition
for k=1:maxk+1
   time(k) = (k-1)*dt;
   for j=1:n+1
      u(1,j,k) =300.*(k<120)+ 70.;
   end
end
%%%%%%%%%%%%%%%%%%%%%%%%%%%%%%%%%%%%%%%%%%%%%%%%%%%%%%%%%%%%%%%%%%%%%%%%%%%%%%%

%   finite difference method computation
for k=1:maxk
   for j = 2:n
      for i = 2:n
         u(i,j,k+1)= alpha*(u(i-1,j,k)+u(i+1,j,k)+u(i,j-1,k)+u(i,j+1,k));

      end
   end
end
% temperature versus space at the final time
```

```
mesh(x,y,u(:,:,maxk)')
figure(3)
mesh(x,time,u(i,j,k+1)')
title('Pressure within the explicit method')
xlabel('y(m)')
ylabel('pressure(Pa)')
```

Figure A Coding of the matrix phase equation using MATLAB

Appendix B

```
clear;
L = 1300;    % length in the x-direction (m)
W = 600;     % length in the y-direction
Tend = 1300.;% final time (Days)
maxk = 2500;
dt = Tend/maxk;
n = 50.;     % Number of space steps

%%%%%%%%%%%%%%%%%%%%%%%%%%%%%%%%%%%%%%%%%%%%%%%%%%%%%%%%%%%%%%%%%%%%%%%%%%%%%%%

% initial condition and part of boundary condition
u(1:n+1,1:n+1,1:maxk+1) = 20*10^6.;
dx = L/n;
dy = W/n;   % use dx = dy = h
h = dx;
b = dt/(h*h);
cond = .002;    % Coefficient of the partial derivative function
spheat = 1.0;   % Constant
rho = 1.;   % density
a = cond/(spheat*rho);
alpha = a*b;
c = 7.8*10^(-5);
for i = 1:n+1
   x(i) =(i-1)*h;   % use dx = dy = h
   y(i) =(i-1)*h;
end
%%%%%%%%%%%%%%%%%%%%%%%%%%%%%%%%%%%%%%%%%%%%%%%%%%%%%%%%%%%%%%%%%%%%%%%%%%%%%%%

% boundary condition
for k=1:maxk+1
   time(k) = (k-1)*dt;
   for j=1:n+1
         end
end
%%%%%%%%%%%%%%%%%%%%%%%%%%%%%%%%%%%%%%%%%%%%%%%%%%%%%%%%%%%%%%%%%%%%%%%%%%%%%%%

%   Explicit finite difference method computation
for k=1:maxk
   for j = 2:n
      for i = 2:n
         u(i,j,k+1)= alpha*(u(i-1,j,k)+u(i+1,j,k)+u(i,j-1,k)+u(i,j+1,k));
      end
   end
end
% Pressure versus space at the final time
mesh(x,y,u(:,:,maxk)')
title('Pressure within the explicit method')
xlabel('y(m)')
zlabel('Pressure(Pa)')
```

Figure B Coding of the natural fractures equation using MATLAB

Appendix C

```
clc
clear
% Matlab Program 5: Diffusion in one dimensional Stimulated Gas Reservoir %within the
% Explicit Method
clear;

% Parameters to define the HYDRAULIC FRACTURE PHASE's equation and the range in space
and time
L = 1300.; % Length of the Stimulated Gas Reservoir (SGR) (m)
T =20*10^3; % Final time (days)
%%%%%%%%%%%%%%%%%%%%%%%%%%%%%%%%%%%%%%%%%%%%%%%%%%%%%%%%%%%%%%%%%%%%%%%%%%%%%%%

% Parameters needed to solve the equation within the explicit method
timek = 2500; % Number of time steps
dt = T/timek;
nn = 50; % Number of space steps
dx = L/nn;
cond = 1/4; % Conductivity
b = 6.241*10^(-9); % Stability parameter (b=<1)
%%%%%%%%%%%%%%%%%%%%%%%%%%%%%%%%%%%%%%%%%%%%%%%%%%%%%%%%%%%%%%%%%%%%%%%%%%%%%%%

% Initial pressure of the SGR: a sinus.
for i = 1:nn+1
x(i) =(i-1)*dx;
p(i,1) =sin(pi*x(i));
end
% Pressure at the boundary (P=0)
for k=1:timek
p(1,k) = 0.;
p(nn+1,k) = 0.;
time(k) = (k-1)*dt;
end
%%%%%%%%%%%%%%%%%%%%%%%%%%%%%%%%%%%%%%%%%%%%%%%%%%%%%%%%%%%%%%%%%%%%%%%%%%%%%%%

% Implementation of the explicit method
for k=1:timek % Time Loop
for i=2:nn; %   Space Loop
p(i,k+1) =p(i,k) + b*(p(i-1,k)+p(i+1,k)-2.*p(i,k))+dt*(3.897*10^(-12)*(20*10^6-
p(i,k))-6.44*10^(-7));
end
end
%%%%%%%%%%%%%%%%%%%%%%%%%%%%%%%%%%%%%%%%%%%%%%%%%%%%%%%%%%%%%%%%%%%%%%%%%%%%%%%

% Graphical representation of the pressure
figure(1)
plot(x,p(:,1),'-',x,p(:,500),'-',x,p(:,800),'-',x,p(:,1200),'-')
title('Pressure behaviour')
xlabel('y(m)')
ylabel('Pressure(Pa)')
ylim([0 2])
```

Figure C Coding of the hydraulic fractures equation using MATLAB